

WI-TR-94-2003

AD-A278 968

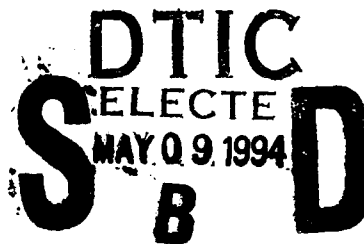


**ADVANCED THERMALLY STABLE, COAL-DERIVED,
JET FUELS DEVELOPMENT PROGRAM ANNUAL REPORT**

EXPERIMENT SYSTEM AND MODEL DEVELOPMENT

**Elmer A. Klavetter
Stephen J. Martin
Wayne M. Trott
Timothy J. O'Hern**

**Sandia National Laboratories
Albuquerque, NM 87185**



December 1993



ANNUAL REPORT FOR THE PERIOD OCTOBER 1992 - SEPTEMBER 1993

APPROVED FOR PUBLIC RELEASE; DISTRIBUTION IS UNLIMITED

**AERO PROPULSION AND POWER DIRECTORATE
WRIGHT LABORATORY
AIR FORCE MATERIEL COMMAND
WRIGHT-PATTERSON AFB, OH 45433-7251**

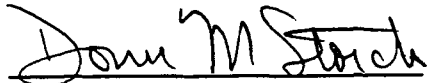
91 5 66 049

Notice

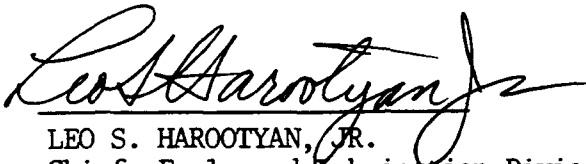
When Government drawings, specifications, or other data are used for any purpose other than in connection with a definitely Government-related procurement, the United States Government incurs no responsibility or any obligation whatsoever. The fact that the government may have formulated or in any way supplied the said drawings, specifications, or other data, is not to be regarded by implication, or otherwise in any manner construed, as licensing the holder, or any other person or corporation; or as conveying any rights or permission to manufacture, use, or sell any patented invention that may in any way be related thereto.

This report is releasable to the National Technical Information Service (NTIS). At NTIS, it will be available to the general public, including foreign nations.

This technical report has been reviewed and is approved for publication.



DONN M. STORCH, Major, USAF
Assistant Chief
Fuels and Lubrication Division
Aero Propulsion and Power Directorate



LEO S. HAROOTYAN, JR.
Chief, Fuels and Lubrication Division
Aero Propulsion and Power Directorate

If your address has changed, if you wish to be removed from our mailing list, or if the addressee is no longer employed by your organization please notify WL/POS, WPAFB, OH 45433-7103 to help us maintain a current mailing list.

Copies of this report should not be returned unless return is required by security considerations, contractual obligations, or notice on a specified document.

| REPORT DOCUMENTATION PAGE | | | Form Approved OMB No. 0704-0188 | |
|---|---|--|---|---|
| Public reporting burden for this collection of information is estimated to average 1 hour per response, including the time for reviewing instructions, searching existing data sources, gathering and maintaining the data needed, and completing and reviewing the collection of information. Send comments regarding this burden estimate or any other aspect of this collection of information, including suggestions for reducing this burden, to Washington Headquarters Services, Directorate for Information Operations and Reports, 1215 Jefferson Davis Highway, Suite 1204, Arlington, VA 22202-4302, and to the Office of Management and Budget, Paperwork Reduction Project (0704-0188), Washington, DC 20503. | | | | |
| 1. AGENCY USE ONLY (Leave blank) | | 2. REPORT DATE December 1993 | | 3. REPORT TYPE AND DATES COVERED Interim; 10/92-9/93 |
| 4. TITLE AND SUBTITLE Advanced Thermally Stable, Coal-Derived, Jet Fuels Development Program Annual Report - Experiment System and Model Development | | | 5. FUNDING NUMBERS C: MI PR1455-91 N-0638 PE: 62203 PR: 3048 TA: 05 WV: 87 | |
| 6. AUTHOR(S) E. A. Klavetter, S. J. Martin, W. Trott, and T. J. O'Hern | | | | |
| 7. PERFORMING ORGANIZATION NAME(S) AND ADDRESS(ES) Sandia National Laboratories P. O. Box 5800 Albuquerque, NM 87185 | | | 8. PERFORMING ORGANIZATION REPORT NUMBER | |
| 9. SPONSORING / MONITORING AGENCY NAME(S) AND ADDRESS(ES) Aero Propulsion and Power Directorate Air Force Materiel Command Wright Laboratory WL/POSF Wright-Patterson Air Force Base, OH 45433-7103 | | | 10. SPONSORING / MONITORING AGENCY REPORT NUMBER WL-TR-94-2003 | |
| 11. SUPPLEMENTARY NOTES | | | | |
| 12a. DISTRIBUTION / AVAILABILITY STATEMENT Approved for public release; distribution is unlimited | | | 12b. DISTRIBUTION CODE | |
| 13. ABSTRACT (Maximum 200 words) A program entitled "Thermally Stable Jet Fuels Development" was initiated in FY89 by the U.S. Air Force, Aero Propulsion and Power Directorate, working jointly with the Department of Energy, Pittsburgh Energy Technology Center. Thermal stability of aviation fuels is of concern because of the potential operation problems arising from fuel degradation under thermal stress conditions. Sandia National Laboratories has been conducting efforts to develop instrumentation for monitoring characteristics of jet fuel degradation and solids deposition and develop models of those mechanisms from the data acquired using that instrumentation. This report describes the instrumentation development, data acquisition, and model parameter determination. | | | | |
| 14. SUBJECT TERMS Jet fuels, thermal stability, fuel degradation, mass sensor, particle formation, quartz crystal microbalance, photon correlation spectroscopy instrumentation | | | 15. NUMBER OF PAGES | |
| | | | 16. PRICE CODE | |
| 17. SECURITY CLASSIFICATION OF REPORT Unclassified | 18. SECURITY CLASSIFICATION OF THIS PAGE Unclassified | 19. SECURITY CLASSIFICATION OF ABSTRACT Unclassified | 20. LIMITATION OF ABSTRACT UL | |

DISCLAIMER

This report was prepared as an account of work sponsored by the United States Government. Neither the United States nor any agency thereof, nor any of their employees, makes any warranty, expressed or implied, or assumes any legal liability or responsibility for the accuracy, completeness, or usefulness of any information, apparatus, product, or process disclosed, or represents that its use would not infringe privately owned rights. Reference herein to any specific commercial product, process or service by trade name, mark, manufacturer, or otherwise, does not necessarily constitute or imply its endorsement, recommendation, or favoring by the United States Government or any agency thereof. The views and opinions of authors expressed herein do not necessarily state or reflect those of the United States Government or any agency thereof.

| | |
|--------------------|--|
| Accession For | |
| NTIS GRA&I | <input checked="checked" type="checkbox"/> |
| DTIC TAB | <input type="checkbox"/> |
| Unannounced | <input type="checkbox"/> |
| Justification | |
| By | |
| Distribution/ | |
| Availability Codes | |
| Dist. | Avail and/or Special |
| A-1 | |

FORWORD

In May 1989, the Fuels Branch of the Aero Propulsion Directorate at Wright-Patterson Air Force Base, Ohio, commenced an investigation to develop advanced, thermally stable jet fuels as well as physical and computer models that could simulate the thermal degradation of those fuels under operational conditions. Funding was provided to the Department of Energy (DOE) Pittsburgh Energy Technology Center (PETC) to administer this effort. This report details efforts of Sandia National Laboratories (SNL), a prime contractor to DOE (DOE Contract #DE-AC04-94AL85000). Development and testing of diagnostic instrumentation systems and analyses of jet fuel liquids and formed solids are described. Mr. William E. Harrison III was the Air Force Program Manager and Mr. Shelby Rogers was the DOE/PETC Program Manager.

TABLE OF CONTENTS

| | | |
|-------|---|------|
| | List of Figures | vi |
| | List of Tables..... | viii |
| 1. | Introduction | 1 |
| 2. | Experimental System Development..... | 1 |
| 2.1 | Development of QCM Jet Fuel Testing Technology..... | 1 |
| 2.1.1 | Second Generation Jet Fuel Test System..... | 1 |
| 2.1.2 | Setup of Jet Fuel Test Systems | 4 |
| 2.1.3 | Development of Oscillator Circuitry..... | 4 |
| 2.1.4 | Software Modifications to Extract Liquid Density Viscosity Product | 5 |
| 2.1.5 | Compensating QCM Response to Changes in Liquid Properties | 7 |
| 2.1.6 | Dual QCM for Liquid Density and Viscosity Extraction..... | 9 |
| 2.1.7 | Additional Information on Operational Capabilities of the QCM-JFTS..... | 13 |
| 2.1.8 | Flow-Thru Jet Fuel Test System | 15 |
| 2.1.9 | Future Work Planned..... | 19 |
| 2.2 | Photon Correlation Spectroscopy System Development and Testing | 19 |
| 2.2.1 | PCS System Description..... | 20 |
| 2.2.2 | PCS Studies of Different Aviation Fuels..... | 20 |
| 2.2.3 | Diffusion Coefficients | 38 |
| 2.2.4 | Refractive Index Measurements | 44 |
| 2.2.5 | Integration of PCS and QCM Techniques | 44 |
| 2.2.6 | Relative Mass Calculations | 49 |
| 3. | Conclusions | 49 |
| 4. | Bibliography | 51 |

LIST OF FIGURES

1. Schematic of QCM Jet Fuel Test System (QCM-JFTS).
2. Comparison of viscosity-density values calculated from QCM measurements for Jet A 92-POSF-2922 with literature values from Coordinating Research Council data.
3. Density-viscosity product of butanol changes vs. temperature (upper graph). Comparison of areal mass density versus temperature for uncompensated and temperature-compensated QCM measurements (lower graph).
4. Imposed sinusoidal temperature variation on fuel (upper graph). Comparison of areal mass density versus time for uncompensated and temperature-compensated QCM measurements (lower graph).
5. Schematic of dual QCM sensor device capable of resolving density and viscosity values of contacting liquid.
6. SEM micrograph of a cross section of the corrugated surface of one QCM sensor in the dual QCM sensor device.
7. Density-viscosity scatter diagram comparing measurements from dual QCM device with literature values.
8. Schematic of flow-thru system for QCM mass deposition measurements.
9. Schematic of first-generation flow-thru QCM cell.
10. Example of mass deposition data versus time for static-flow and flow-thru cell.
11. Schematic representation of PCS system for studies of heated jet fuels.
12. Particle growth rates measured by PCS for two fuels heated to 160°C.
13. Normalized scattered light intensity for two fuels heated to 160°C.
14. Particle growth rates measured by PCS for three fuels heated to 150°C.
15. Normalized scattered light intensity for three fuels heated to 150°C.
16. Particle growth rates measured by PCS for two fuels heated to 140°C.
17. Normalized scattered light intensity for two fuels heated to 140°C.

18. Particle diameters as a function of temperature and exposure time in Jet A 91-POSF-2827.
19. Particle diameters as a function of temperature and exposure time in Jet A 92-POSF-2922.
20. Induction times for detectable particle formation in Jet A 92-POSF-2922 as measured by PCS. Circles indicate the time required for mean particle diameter to reach 200 nm, squares the extrapolated time for particles to appear ("0 nm"--see Figure 19).
21. Arrhenius-type plot of PCS-measured particle growth rate in Jet A 92-POSF-2922.
22. Real-time measurements of particle size distributions during 145°C heating of Jet A 92-POSF-2922.
23. Effect of oxygen saturation on PCS-measured particle growth rate in Jet A 92-POSF-2922 heated to 150°C.
24. QCM mass deposition data in Jet A 91-POSF-2827 heated to 150°C. Test performed in PCS experimental set-up.
25. QCM mass deposition data in Jet A 92-POSF-2922 heated to 160°C. Test performed in PCS experimental set-up.
26. Particle growth rates measured by PCS in Jet A 91-POSF-2827. Comparison of three runs at 150°C (with and without QCM in cell).
27. Relative mass of particles in Jet A 91-POSF-2827 heated to 160°C (see text for description of calculation method).

LIST OF TABLES

1. Sulfur and Nitrogen Analysis of Three Aviation Fuels.
2. Particle Sizes in Post-Stressed Fuels.
3. Particle Diameter and Diffusion Coefficient for Various Stress Temperatures.

ACKNOWLEDGEMENTS

This project was jointly supported by the U.S. Department of Energy, Pittsburgh Energy Technology Center (PETC) and the Aero Propulsion and Power Directorate, Wright-Patterson Air Force Base, Ohio. This work was supported by the U.S. Department of Energy at Sandia National Laboratories under Contract #DE-AC04-94AL85000. The authors wish to express their appreciation to Mr. S. Rogers (PETC) and Mr. W. E. Harrison III, Major D. Storch and Dr. W. M. Roquemore (Aero Propulsion and Power Directorate) for their support of this effort.

I. Introduction

Thermal stability of aviation fuels is of concern because of potential operational problems arising from fuel degradation under thermal stress conditions. Hydrocarbon fuels in contact with heated metallic surfaces form insoluble, carbonaceous deposits that can foul nozzles, manifolds, filters, injectors, and heat exchangers. Sandia National Laboratories, Albuquerque, is part of a U.S. Air Force, Wright Laboratory, program, to investigate thermal stability characteristics of current aviation fuels and develop fuels with enhanced thermal stability characteristics. For these investigations, measurement techniques are required which can monitor the degradation processes as the fuel is thermally stressed. Sandia is developing two instrumentation systems which have the capability to monitor important fuel degradation processes: (1) the formation and growth of particles resulting from fuel oxidation or pyrolytic reactions, and (2) the deposition of the produced solids on metal surfaces. This document discusses the current state of development of these instrumentation systems and presents typical results that can be obtained by these systems under temperature and time conditions representative of those experienced by the fuel in an aviation fuel system.

2. Experimental System Development

2.1 Development of QCM Jet Fuel Testing Technology

This section of the report will address the development of the quartz crystal microbalance (QCM) sensor technology for monitoring deposition of solids onto surfaces in contact with jet fuel. We describe the status of the QCM technology as integrated into both a static-cell and flowing-cell test system. Improvements to the operational capability of the system are also discussed.

2.1.1. Second Generation Jet Fuel Test System

Last year we reported on the development of a "second generation" QCM-based Jet Fuel Test System (QCM-JFTS) for monitoring deposition of solids onto surfaces in contact with jet fuel during thermal degradation. The most significant advantage of the second generation system was the elimination of the costly network analyzer required in the first generation system. We briefly review the current QCM-JFTS, shown schematically in Fig. 1. The apparatus includes a QCM test fixture to hold the QCM suspended in a jet fuel sample, an oscillator to drive the QCM, a frequency counter and digital voltmeter to monitor the

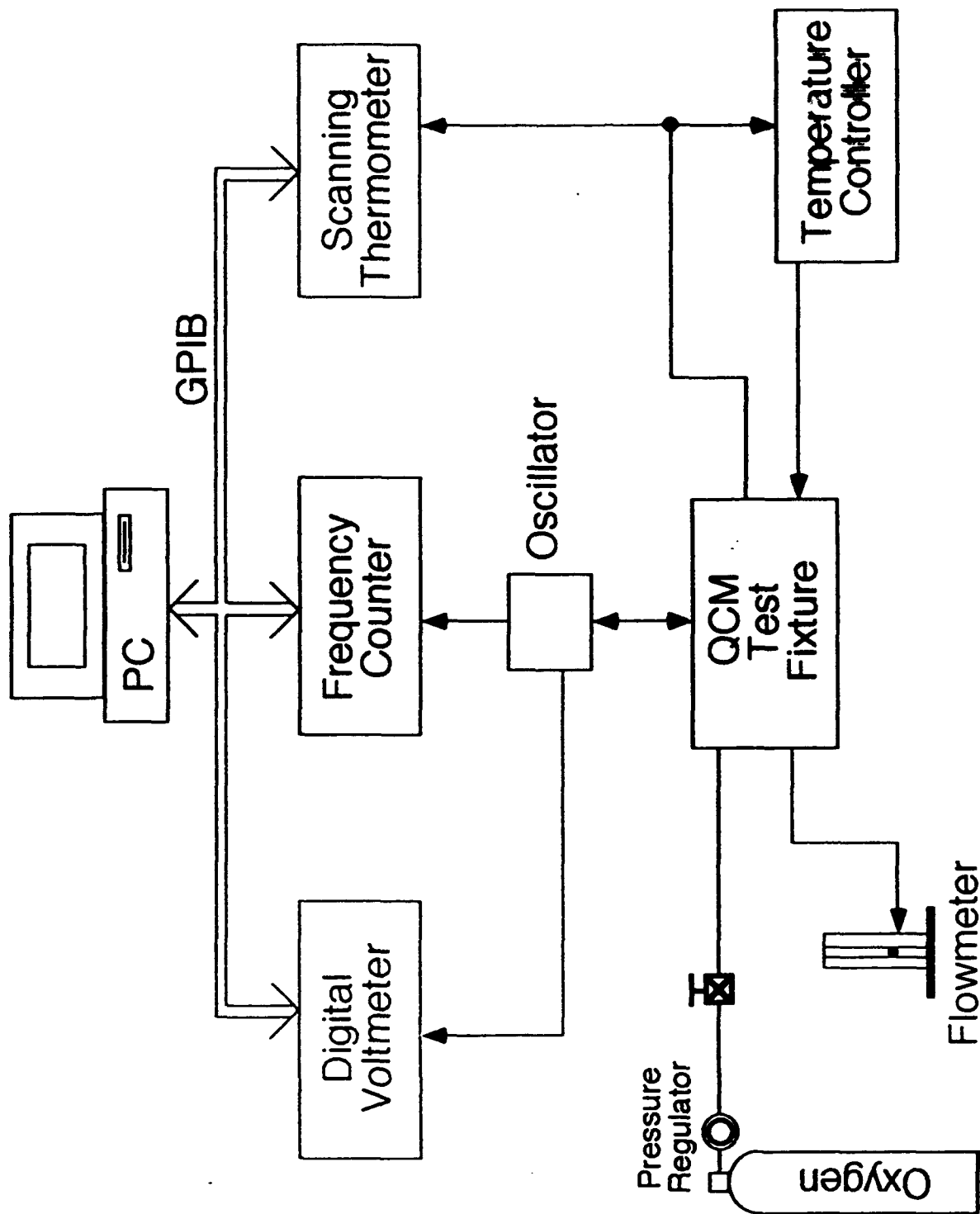


Figure 1. Schematic of WCM Jet Fuel Test System (WCM-JFTS).

oscillator outputs, a temperature controller to maintain sample temperature, a scanning thermometer to read fuel temperature, a gas flow meter, and a personal computer (PC) to acquire and display sensor data.

The QCM test fixture houses the QCM sensor suspended in a sample of jet fuel, allowing mass accumulation to be measured at elevated temperatures and with oxygen overpressures. The test fixture consists of a stainless steel pressure vessel (Parr Instrument Co.) modified to include an RF electrical feedthrough mounted in the lid. A QCM clamp holds the edge of a QCM, making electrical contact to the electrodes. The lid of the test fixture also contains feedthroughs for an oxygen inlet and vent tube, a pressure gauge, a pressure relief valve, and a thermocouple. The lid seals to the body of the vessel with a teflon gasket and clamps, allowing oxygen overpressures of up to 1000 psi to be maintained during the test. The QCM test fixture is mounted in a band heater, allowing test temperatures up to 300°C to be achieved. In addition, the unit is suspended by a clamp stand above a magnetic stirrer, allowing the fuel sample to be mixed during the test, maintaining a uniform temperature and oxygen concentration.

A key component of the second generation QCM-JFTS is an oscillator circuit that drives the quartz resonator suspended in jet fuel. This circuit uses the impedance variations inherent in the QCM resonant response to track the resonance frequency of the sensor. Because of the severe operating environment, commercial oscillators proved inadequate. Consequently, an oscillator was custom-designed at Sandia National Laboratories for this application. The oscillator board is unique in providing outputs of both resonant frequency and crystal damping.

The oscillator frequency output is read by a frequency counter (HP model 5384A) and input to the PC as an indicator of mass accumulation. The mass density, ρ_s (mass/area) accumulated on each crystal face is related to the change in resonant frequency Δf (measured at constant temperature) by:

$$\rho_s = -c_1 \Delta f \quad (1)$$

where $c_1 = 8.84 \times 10^{-3}$ g-s/cm² for a 5 MHz QCM.

Interpreting frequency changes in terms of mass accumulation according to Eq. 1 will be erroneous if the fuel and crystal temperatures are varying, since fuel viscosity will vary with temperature and contribute a frequency change also. In addition, the resonant frequency of the crystal itself has some slight temperature dependence. These problems have been addressed in the past year. Improvements have been made in the algorithm for determining

mass deposition which accounts for changes in fluid properties. We will show below that the erroneous contribution to the mass reading arising from these changes can be largely eliminated.

A temperature controller (Parr model 4842) reads the thermocouple in contact with jet fuel and controls current flow to the band heater in order to maintain the jet fuel at a constant test temperature. A scanning thermometer also reads the thermocouple contacting the jet fuel and sends this information to the PC.

The personal computer acquires data during the test, displaying it in real time and storing it for later use. The PC communicates with the digital voltmeter, frequency counter, and scanning thermometer via a parallel interface bus (GPIB). A user-friendly program running in a windows environment displays a "control panel" for controlling the test and monitoring the data in real time. The program is a Sandia proprietary program written in the *HP Instrument Basic for Windows* program environment.

2.1.2 Set-up of Jet Fuel Test Systems

Four Jet Fuel Test Systems of the type described above were delivered and set up for the Air Force this past year. Two systems were installed for Wright Laboratory, a third system was set up for the University of Dayton Research Institute (UDRI) and one was set up for Pratt & Whitney, Inc. (West Palm Beach, FL). Operators were instructed on the use of the systems and have successfully operated these systems to evaluate jet fuel degradation. One system was modified by Steve Zabarnick of the UDRI to include a pressure transducer in the reaction vessel. A pressure transducer has now been included in the standard Sandia test system design.

2.1.3 Development of Oscillator Circuitry

The oscillator circuit used to operate the QCM sensor in jet fuel has been substantially improved this year. The motional resistance range that the circuit can tolerate has been increased to 3500 Ohms, enabling the sensor to be operated in more viscous fluids. Previously, the device could only be operated in liquids with a density-viscosity product up to $5.3 \text{ g}^2\text{cm}^4\text{s}^{-1}$. By increasing the maximum transconductance of the oscillator circuit and tuning out the shunt capacitance of the resonator fixture, the sensor can now be operated in liquids with density-viscosity products up to $20.3 \text{ g}^2\text{cm}^4\text{s}^{-1}$. This nearly fourfold increase allows mass accumulations to be measured in more viscous fluids as well as enabling fluid properties to be measured (described below) over a wider range. In previous tests with some

jet fuels (e.g., JP-7), the oscillator would not function at ambient temperature because of the higher viscosity value for the fuel compared to standard Jet A fuels. The oscillator would begin to function as the temperature was raised (usually to about 50°C) and the viscosity of the fuel correspondingly decreased. Because fuels of improved thermal stability may have higher viscosities than current fuels, the oscillator was modified to resolve this potential limitation.

2.1.4 Software Modifications to Extract Liquid Density-Viscosity Product

The oscillator board provides both a resonant frequency and crystal damping output. Crystal damping is given in terms of the motional resistance R_2 of the crystal, related to liquid density and viscosity by:

$$R_2 = c_3 (\rho\eta)^{1/2} \quad (2)$$

where c_3 is a constant.

The QCM-JFTS software has been modified to use the damping output R_2 from the oscillator circuit to indicate the density-viscosity product of a fluid contacting the QCM sensor. Because this determination depends on the characteristics of the individual oscillator circuit used with the QCM sensor, a routine has been included in the software that permits the operator to place a "calibration fluid" (butanol has been chosen as the calibration fluid at this time; options for different calibration fluids will be incorporated at a later time) in contact with the sensor and determine the relationship between damping voltage and the fluid density-viscosity product. The system measures QCM damping and fluid temperature. From the known dependence of fluid properties on temperature, the program calibrates the damping measurement in terms of the fluid density-viscosity product. With this addition, the QCM-JFTS can measure both surface mass accumulation as well as the density-viscosity product ($\rho\eta$) of the contacting jet fuel.

Fig. 2 shows the density-viscosity product of Jet A fuel 92-POSF-2922 extracted from QCM measurements along with literature values of the density-viscosity product (CRC). Reasonable agreement is found between the two. Viscosity values for other fuels at discrete temperatures are discussed in Section 2.2.

JF 2922 Viscosity-Density Data

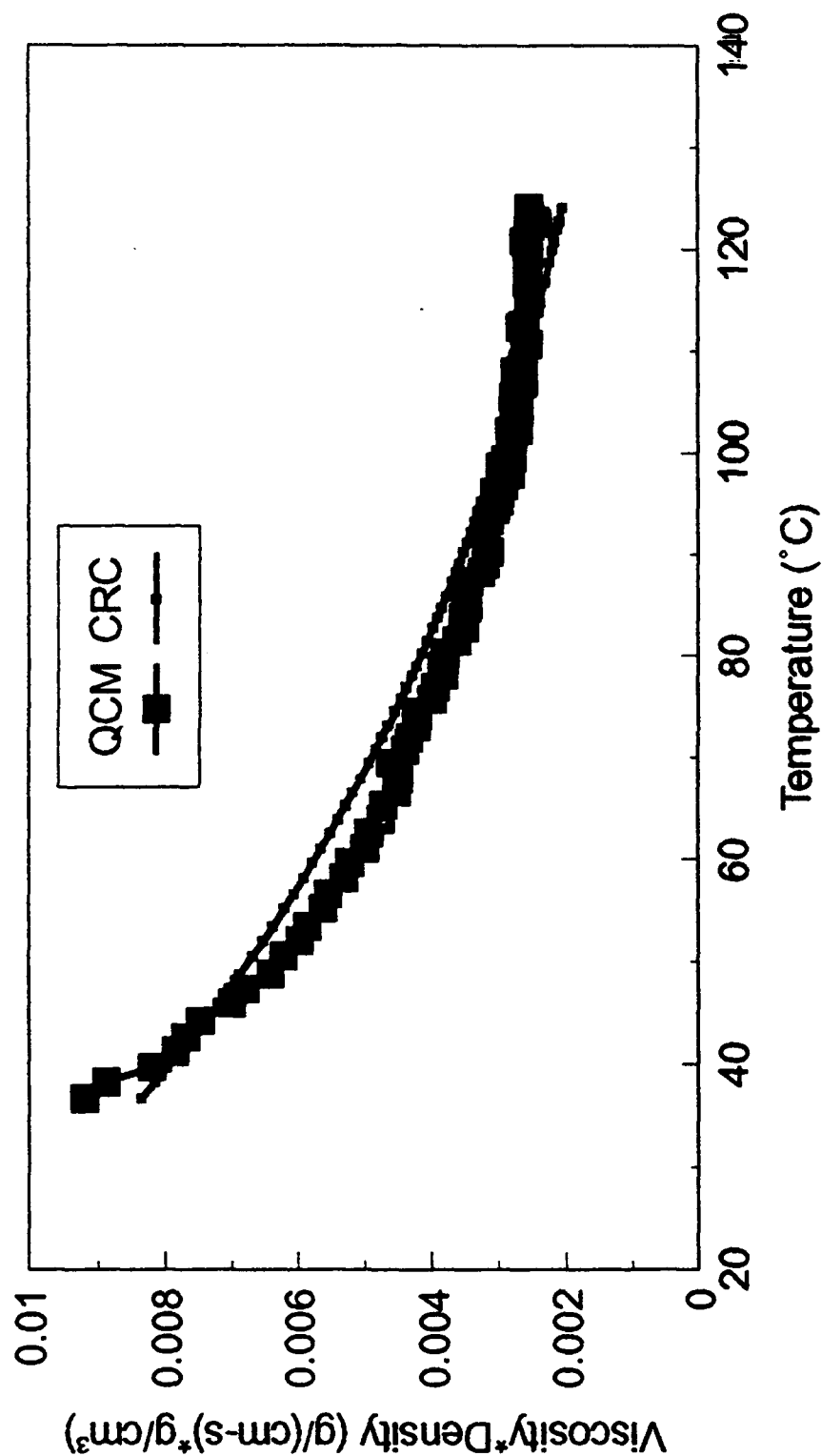


Figure 2. Comparison of viscosity-density values calculated from QCM measurements for Jet A92-POSF-2922 with literature values from Coordinating Research Council data.

2.1.5 Compensating QCM Response for Changes in Liquid Properties

One of the limitations in measuring solid deposition using the QCM sensor has been the need to make measurements at constant temperature. This is due to the fact that the QCM resonant frequency is sensitive not only to surface mass but also to properties of the contacting liquid. We have shown that when a QCM is immersed in liquid, its resonant frequency changes as:

$$\Delta f = -c_1 \rho_s - c_2 (\rho \eta)^{1/2} \quad (3)$$

where c_1 and c_2 are constants, ρ_s is the surface mass density (mass/area), while ρ and η are liquid density and viscosity. Eq. 3 indicates that changes in fluid density and/or viscosity will cause a change in resonant frequency, Δf . If Eq. 1 is used, which interprets the frequency change exclusively as surface mass accumulation, this change in liquid properties will give an erroneous mass reading.

Since the damping output from the oscillator circuit is proportional to $(\rho \eta)^{1/2}$ (Eq. 2), crystal damping measurements can be used to indicate changes in fluid properties and correct Δf for this contribution. Combining Eqs. 2 and 3 gives:

$$\rho_s = -\frac{\Delta f + c_2' \Delta R_2}{c_1} \quad (4)$$

By calculating mass accumulation using *both* Δf and ΔR_2 , according to Eq. 4, rather than from Δf alone (Eq. 1), the effect of changes in liquid properties can be minimized. The system is calibrated by placing the QCM in contact with the calibration fluid (e.g., butanol) and measuring Δf and ΔR_2 while varying temperature. As liquid properties vary with temperature, the ratio of the frequency to damping changes determines c_2' :

$$c_2' = -\frac{\Delta f}{\Delta R_2} \cong \frac{8.4 \text{ kHz}}{V} \quad (5)$$

Fig 3 shows how the density-viscosity product of butanol changes vs. temperature (upper) and a comparison in the mass registered (lower) for an uncompensated QCM measurement (Eq. 1) and one using the compensation scheme outlined above (Eqs. 4 and 5).

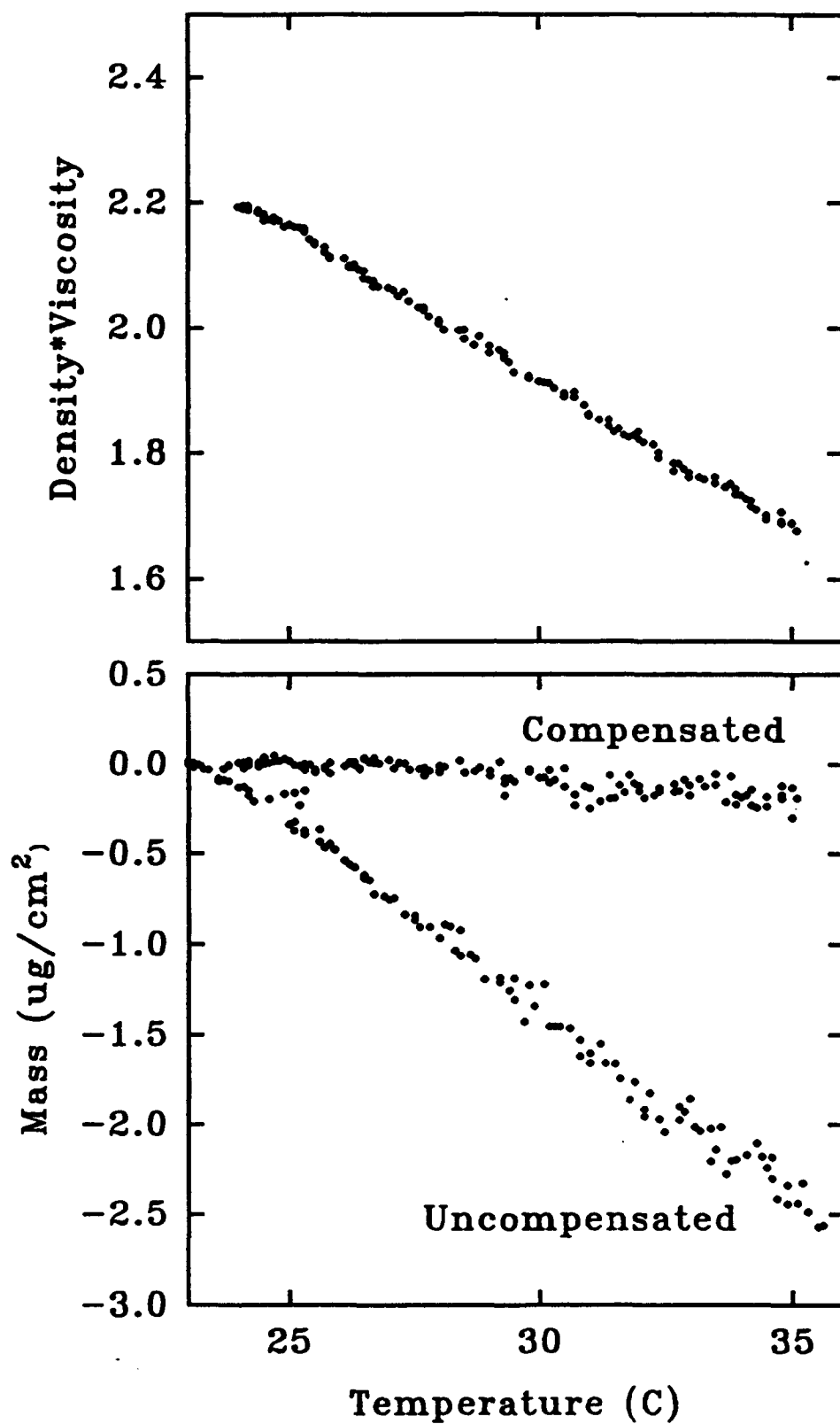


Figure 3. Density-viscosity product of butanol changes vs. temperature (upper graph). Comparison of areal mass density versus temperature for uncompensated and temperature-compensated QCM measurements (lower graph).

The uncompensated device registers an erroneous mass loss of $2.5 \mu\text{g}/\text{cm}^2$, while the compensated device registers negligible mass change.

The compensation scheme has also been examined during cyclical temperature variations of jet fuel in contact with a QCM. Fig. 4 (upper) shows a sinusoidal temperature variation imposed on JET A 91-POSF-2827 fuel sparged with N_2 to minimize mass deposition. The lower plot shows the mass registered. The uncompensated measurement shows a sinusoidally-varying mass error, while the compensated measurement shows no sinusoidal mass error. The compensated measurement is somewhat noisy, due to a noisy voltage measurement of R_2 . This noise level can presumably be reduced by averaging a number of measurements.

The data indicate that the sensitivity of the QCM mass indication to fluctuations in fluid properties, typically induced by temperature changes, can be reduced by using the damping measurement to correct for fluid property changes.

2.1.6 Dual QCM for Liquid Density and Viscosity Extraction

It is apparent from Eqs. 2 and 3 that liquid properties enter into the response of a smooth-surfaced QCM only as the product of density and viscosity ($\rho\eta$). This year a new device has been developed that is capable of individually resolving the density and viscosity of a contacting fluid. This device, shown in Fig. 5, consists of a pair of quartz resonators fabricated together as a monolithic quartz sensor. Because liquid viscosity is very temperature dependent, a serpentine resistance temperature device (RTD) is also fabricated on the quartz die to determine the temperature of the liquid under test. This type of device modification may be required when the temperature of the fuel is changing significantly near the QCM sensor location.

The pair of quartz resonators has one with a smooth surface and one with a corrugated surface. Fig. 6 shows a SEM micrograph of a cross section of the corrugated device surface. Photoresist strips were patterned on the surface, followed by electrodeposition of gold, to form the $5\text{-}\mu\text{m}$ -wide surface ridges. These ridges serve to confine a precise quantity of liquid at the surface. The difference in texture between the smooth and corrugated devices causes them to respond differently to liquid density and viscosity and allows extraction of both parameters. (Solid deposition from the liquid is not considered at present.)

When the smooth device is contacted by liquid, viscous entrainment of a thin layer of contacting liquid causes the resonant frequency to change by (Eq. 3 with $\rho_s = 0$):

$$\Delta f_1 = -c_2 (\rho\eta)^{1/2} \quad (6)$$

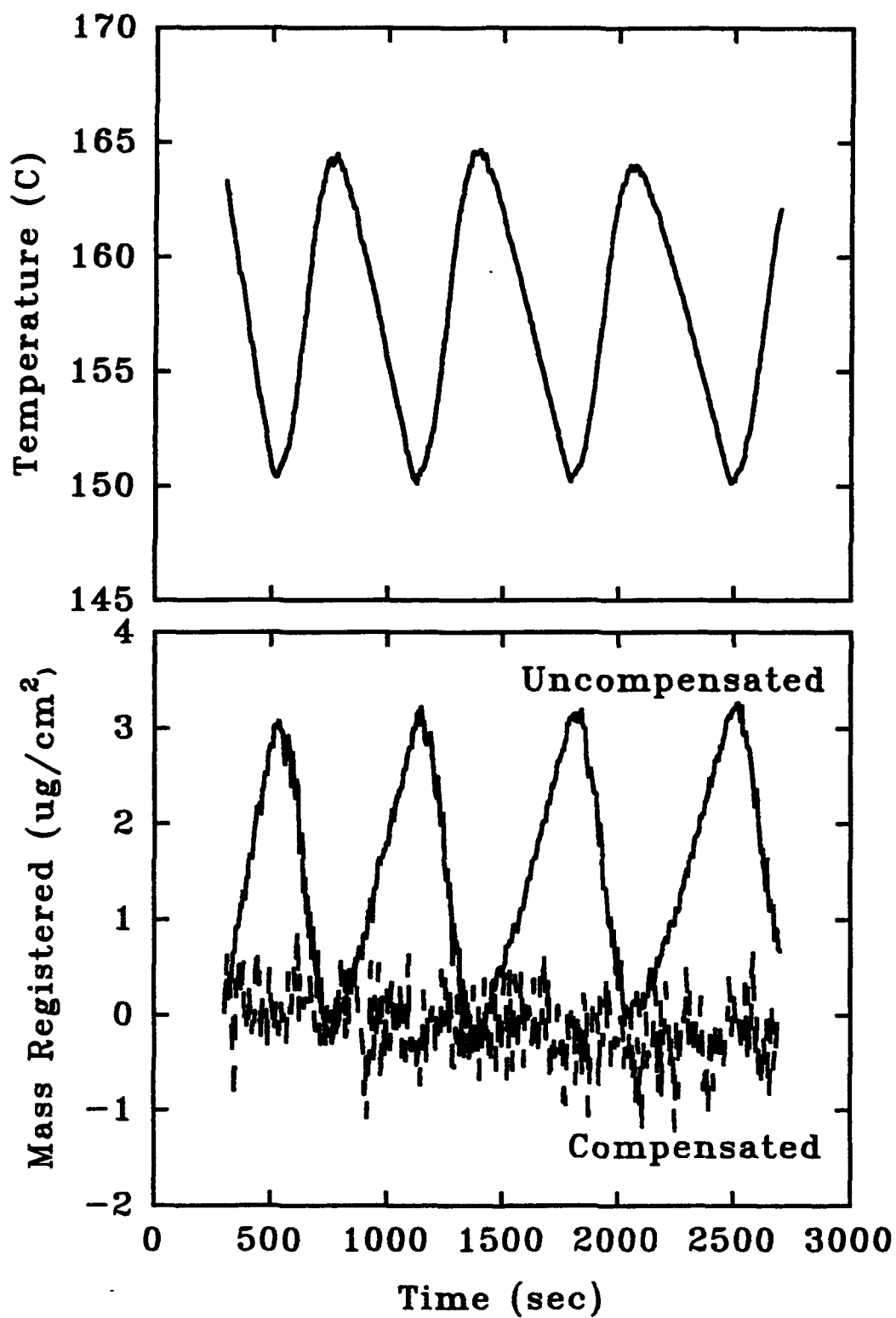


Figure 4. Imposed sinusoidal temperature variation on fuel (upper graph). Comparison of areal mass density versus time for uncompensated and temperature-compensated QCM measurements (lower graph).

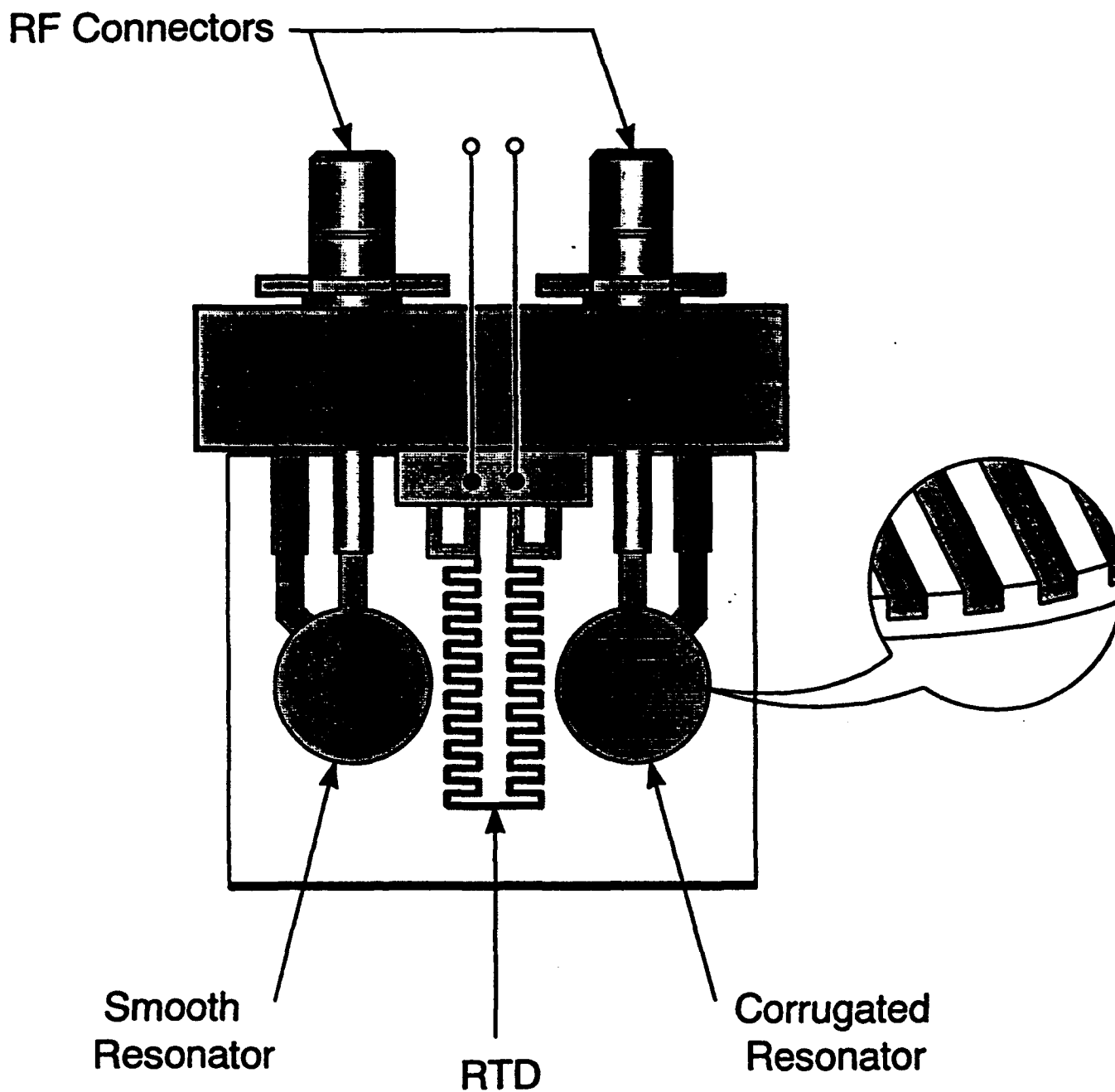


Figure 5. Schematic of dual QCM sensor device capable of resolving density and viscosity values of contacting liquid.

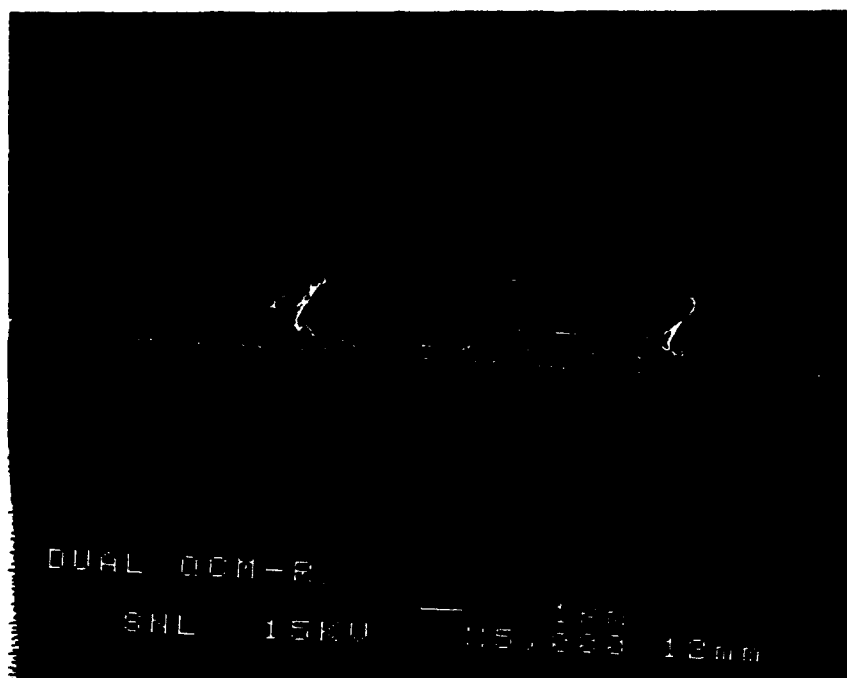


Figure 6. SEM micrograph of a cross section of the corrugated surface of one QCM sensor in the dual QCM sensor device.

The device with the corrugated surface *traps liquid in the surface corrugations* in addition to entraining a liquid layer like the smooth device. This trapped liquid behaves as a mass layer, moving synchronously with the oscillating device. This results in an additional frequency change for the corrugated device proportional to liquid density:

$$\Delta f_2 = -c_2 (\rho\eta)^{1/2} - c_4 \rho h \quad (7)$$

where c_2 and c_4 are constants and h is the corrugation depth (approx. 1.5 μm).

The difference in responses between the smooth and rough devices gives the liquid density:

$$\rho = \frac{\Delta f_1 - \Delta f_2}{c_4 h} \quad (8)$$

Substituting this result into Eq. 6 then gives the liquid viscosity:

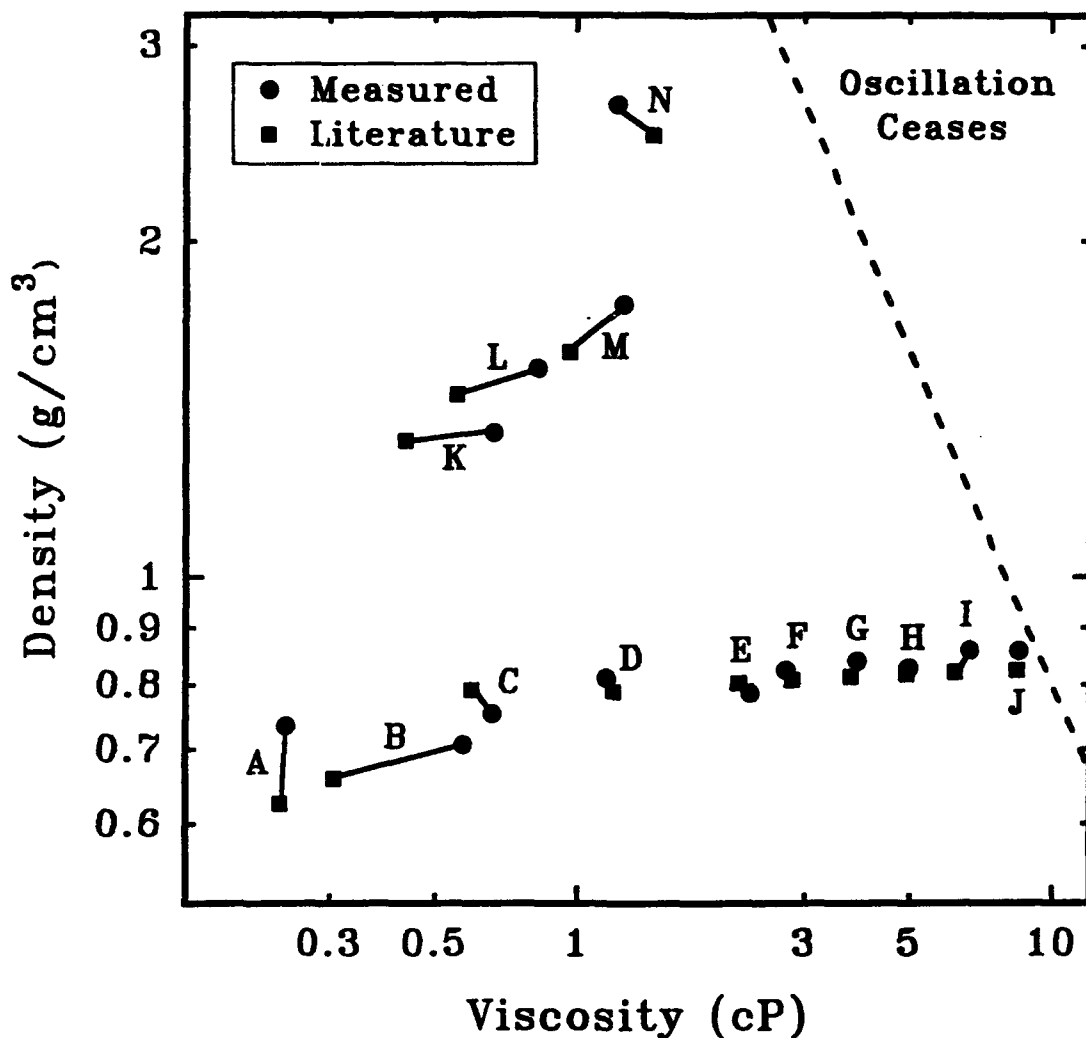
$$\eta = \frac{\Delta f_1^2}{c_2^2 \rho} = \frac{c_4 h}{c_2^2} \frac{\Delta f_1^2}{\Delta f_1 - \Delta f_2} \quad (9)$$

Fig. 7 shows a "scatter diagram" of density and viscosity values extracted for a number of liquids from dual-QCM measurements; literature values for these parameters are shown for comparison.

In addition to monitoring jet fuel properties, the dual-QCM sensor should be useful for a number of liquid monitoring applications. (A patent application has been filed on this invention.) Examples include a state-of-charge indicator for batteries: electrolyte density is indicative of battery charge. An oil condition indicator for automotive use is also under development: oil viscosity indicates the end of lubricant life.

2.1.7 Additional Information on Operational Capabilities of the QCM-JFTS

A variety of tests have been performed to test the range of conditions under which the QCM-JFTS can be operated and data obtained relevant to jet fuel thermal stability. Although current testing generally has occurred at temperatures lower than 200°C and at low pressures (<80 psig), we have checked out the operation of the system at temperatures up to 310°C and pressures up to 575 psig. We pressure-checked the pressure vessel up to 1000 psig but put a pressure relief valve on the system set at 600 psig. If the rf feedthrough is adequately



- | | |
|---------------|-------------------------|
| A. n-Pentane | H. n-Hexanol |
| B. n-Hexane | I. n-Heptanol |
| C. Methanol | J. n-Octanol |
| D. Ethanol | K. Dichloromethane |
| E. n-Propanol | L. Trichloroethylene |
| F. n-Butanol | M. Carbon Tetrachloride |
| G. n-Pentanol | N. Dibromomethane |

Figure 7. Density-viscosity scatter diagram comparing measurements from dual QCM device with literature values.

welded to the reactor, the reactor can theoretically take pressures up to 3000 psig. At this time, we recommend a maximum operating temperature of 300°C and maximum pressure of 550 psig.

We have also tested the system with fluids of much higher viscosity. As noted earlier, the oscillator circuitry was enhanced to permit fluids with viscosity-density values up to $20.3 \text{ g}^2 \text{ cm}^{-4} \text{ s}^{-1}$. Using a network analyzer in place of the oscillator circuitry, fluids with even higher viscosities can be tested. We tested petroleum resid in the pressure vessel at temperatures over 300°C and pressures over 500 psig and were able to accurately measure density-viscosity product values. We believe the range of operability of the system may make it useful in testing other fluids related to aircraft operation (i.e., lubricants).

We have made several runs using Jet A fuels at low and high temperatures. We stressed fuel at 100°C for over 8 days (with a linear deposition rate of $0.1 \text{ } \mu\text{g}/\text{cm}^2\text{-hr}$). We stressed fuel at different temperatures in the range of 200 to 250°C for several hours. In all cases, data were obtained consistent with expectations on rates. A new procedure is required for testing fuels at higher temperatures ($>200^\circ\text{C}$ and perhaps lower) because the available oxygen in the fuel is consumed during the heat-up period. For lower temperature tests, the oxygen consumption is at a sufficiently low rate that oxygen is still available after the heat-up period. Therefore, we recommend that for higher temperature tests where oxygen is required, the fuel be sparged with oxygen at the elevated temperature rather than pre-test. Tests at different temperatures have demonstrated that the fuel may be sparged with oxygen numerous times during thermal stressing without changing the deposition rate.

2.1.8 Flow-Thru Jet Fuel Test System

The measurements reported to date have all been made with a static-flow test cell: a fixed sample of jet fuel was placed in a closed pressure reactor and mass deposition measurements were made on a QCM suspended in this sample. In the past year a flow-thru jet fuel test system was assembled and preliminary measurements were made using it. In this system, shown schematically in Fig. 8, a sample of jet fuel is maintained at elevated temperature and circulated across a QCM sensor housed in a flow-thru test cell. (A $5\text{-}\mu\text{m}$ filter is included to keep particulates from accumulating in the pump.) The flow-thru test cell, shown schematically in Fig. 9, allows mass accumulation to be measured on the QCM from a flowing fuel stream.

In performing tests with the flow-thru test system, a QCM was also placed in the "static cell" (jet fuel reservoir) so that mass deposition rates could be compared between the flow-thru cell and the static cell. Fig. 10 shows mass deposition vs. time for QCMs in the static

Measurement of Mass Deposition with Flow-Thru Cell

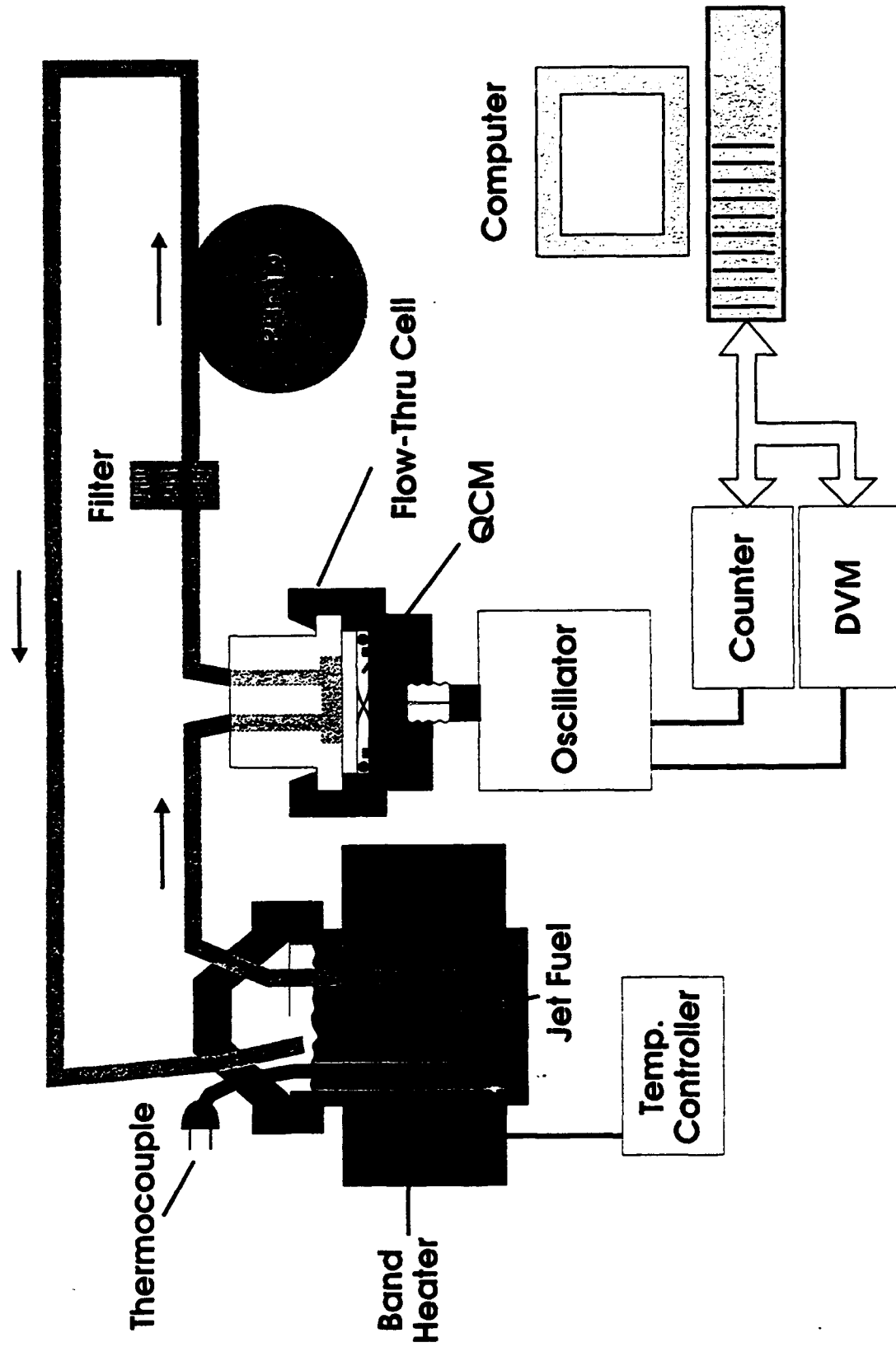


Figure 8. Schematic of flow-thru system for QCM mass deposition measurements.

Flow-Thru QCM Cell

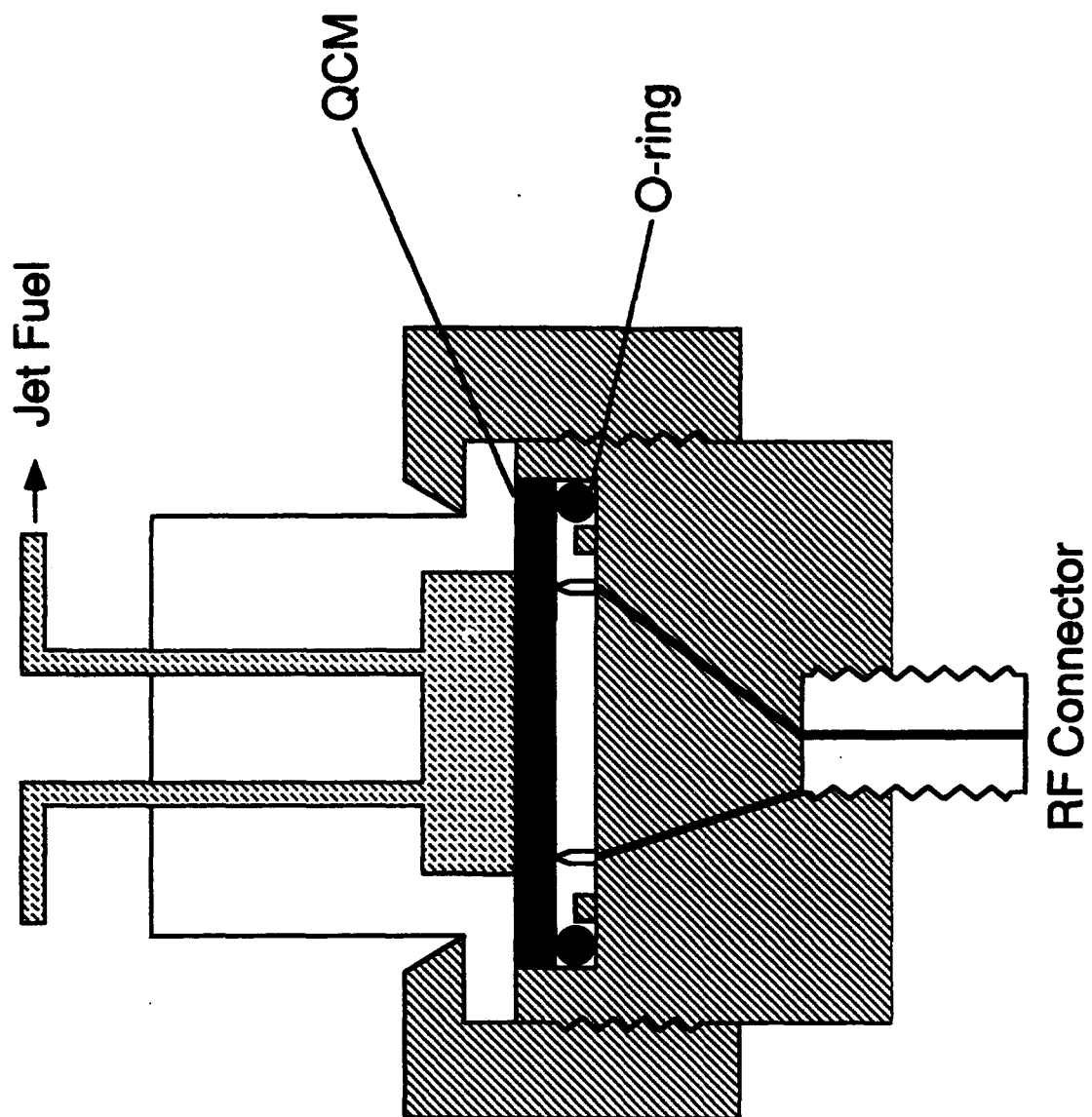


Figure 9. Schematic of first-generation flow-thru QCM cell.

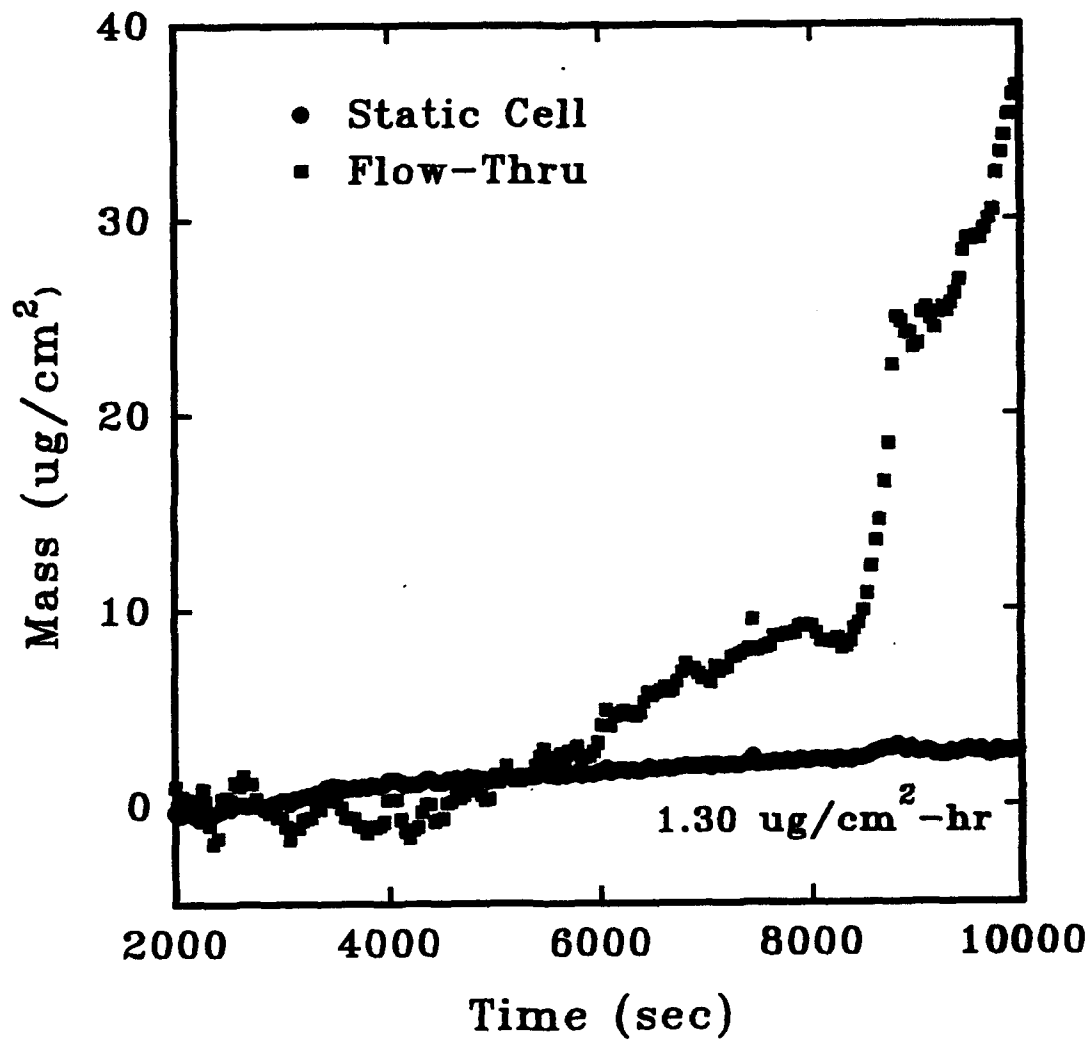


Figure 10. Example of mass deposition data versus time for static-flow and flow-thru cell.

and flow-thru cells. JET A 91-POSF-2827 fuel was oxygenated for 20 minutes and maintained at 170°C in the static cell. The QCM housed in this cell recorded a fairly linear mass accumulation at a rate of 1.30 $\mu\text{g}/\text{cm}^2\text{-hr}$; the QCM in the flow-thru cell, at a somewhat lower temperature, recorded a much higher nonlinear mass accumulation rate. It appears that particulates formed at 170°C in the static cell condense on surfaces more readily in the cooler flow-thru cell. More testing will be performed to evaluate this flow-thru test system concept.

2.1.9 Future Work Planned

Work planned for the next year includes:

- 2.1.9.1 A better assessment will be made of the temperature-compensation scheme outlined above. Experiments will be performed in which depositions are made under conditions of changing fluid temperature and the effectiveness of the compensation scheme evaluated.
- 2.1.9.2 A "third generation" Jet Fuel Test System is under development. This system will use a redesigned reaction chamber that will allow QCMs to be more easily interchanged and smaller fuel sample volumes to be tested. The chamber will incorporate a pressure transducer to monitor oxygen depletion. The system will use internal computer boards to measure oscillator responses and control test temperature and gas flows. This will eliminate the external test instruments (frequency counter, digital voltmeter, multimeter, temperature scanner, and temperature controller) currently used in the test system.
- 2.1.9.3. An improved flow-thru cell will be developed that allows temperature monitoring and control in the cell. The present flow-thru cell has no means of controlling temperature, resulting in a temperature drop in the fuel as it enters the cell.

2.2 Photon Correlation Spectroscopy System Development and Testing

Work over the past year has focused on the use of photon correlation spectroscopy (PCS) for comparison of particle formation characteristics of three different aviation fuels. In

addition, the following tasks have been addressed: (1) determination of diffusion coefficients for particles in heated jet fuels from available PCS data, (2) application of a refractometer for measurement of fuel refractive indices (needed for quantitative analysis of PCS data), (3) preliminary attempts to incorporate a quartz crystal microbalance (QCM) system (for mass deposition measurements) in a PCS test assembly, and (4) calculation of relative masses associated with particle formation in the bulk fuel using Mie intensity parameters in combination with observed scattering intensities and the particle size distributions determined by PCS.

2.2.1 PCS System Description

Of the few techniques available for measurement of submicron diameter particles suspended in a liquid (Weiner, 1984), PCS may be the most suitable for noninvasive, in situ measurement of the small particles generated in jet fuel thermal stability tests. A real-time, in situ diagnostic technique is needed to ensure that particle measurements are made at the desired thermal stress temperature and exposure time as well as to eliminate particle settling effects. The capability of PCS for accurate sizing of small particles is particularly important since much of the relevant fuel degradation chemistry apparently begins in a regime where particle diameters are generally less than a few hundred nanometers (Bolshakov, 1974). A schematic representation of the experimental setup used for the PCS measurements is shown in Fig. 11. PCS uses a digital autocorrelation technique to measure the time-dependent intensity of the scattered light signal caused by Brownian motion of particles in an illuminated sample (Klavetter et al., 1992; Trott et al., 1992). A frequency counter is also employed to acquire a record of the intensity of the scattered light signal (proportional to particle size and concentration) and to ensure that the total photon count rate is appropriate for the correlator sample time (Weiner, 1984). All PCS measurements presented in this report were made at a fixed 90° scattering angle; however, the capability for multiangle scattering measurements is available. System characterization studies, data analysis methods, and early results of PCS tests on heated jet fuels have been documented in Trott et al., 1992 and O'Hern et al., 1993. Detailed general discussions of PCS instrumentation and data reduction methods are also available (Oliver, 1974; Berne and Pecora, 1976; Weiner, 1984).

2.2.2 PCS Studies of Different Aviation Fuels

Photon correlation spectroscopy has been used to examine particle formation in three different specification-grade fuels. The fuels of interest are designated as:

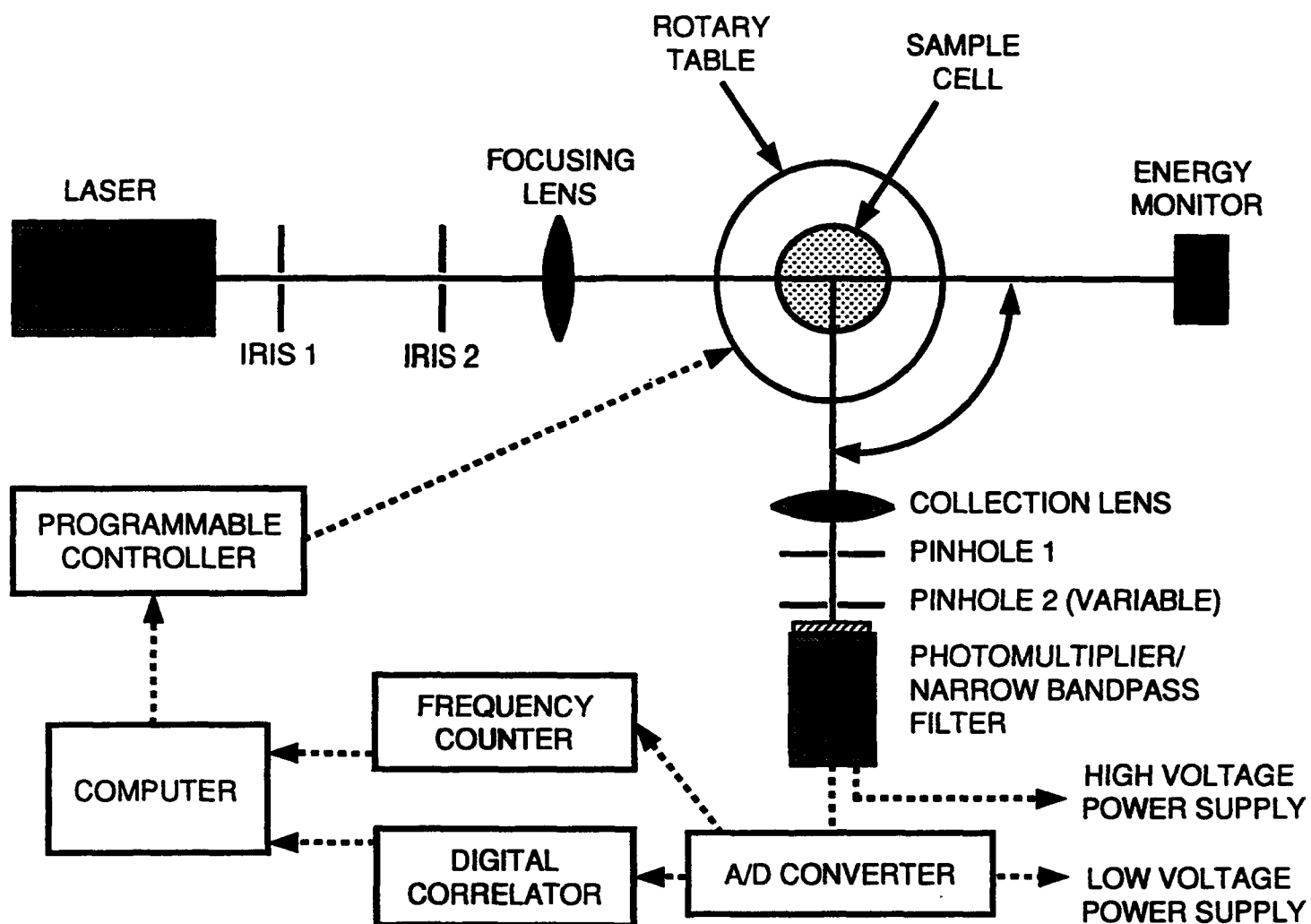


Figure 11. Schematic representation of PCS system for studies of heated jet fuels.

- Jet A-1 90-POSF-2747
- Jet A 91-POSF-2827
- Jet A 92-POSF-2922

The Jet A-1 90-POSF-2747 is a highly hydro-treated fuel and generally exhibits a higher thermal stability than the other two fuels. In addition, sulfur/nitrogen analyses of these three fuels have demonstrated significant differences in some trace constituents, as shown in Table 1. In particular, Jet A 91-POSF-2827 contains a relatively high concentration of sulfur which is known to contribute to particle formation and mass deposition (Heneghan and Harrison, 1992). Substantial differences in the bulk particle formation behavior of the three fuels have been seen in real-time observations of the particle growth rates versus stress temperature, in measurements of the scattered light intensity as a function of both temperature and exposure time, and in post-stress examination of the particle size distribution in samples after cooling.

Table 1: Sulfur/Nitrogen Analysis of Three Aviation Fuels

| Fuel Type | Sulfur | Nitrogen |
|----------------------|---------|----------|
| Jet A-1 90-POSF-2747 | 10 ppm | 60 ppm |
| Jet A 91-POSF-2827 | 660 ppm | 70 ppm |
| Jet A 92-POSF-2922 | 180 ppm | 490 ppm |

For the tests reported here, fuel was prepared by filtering each sample through a 0.2- μ m PTFE filter and then sparging the fuel with oxygen for 15 minutes. In general, oxygen was not continuously supplied during heating; hence, the observed particle growth typically reflects oxygen-deficient conditions. As in previous PCS tests, fuel samples (50 ml) were placed in a sample cell/heater device consisting of an optical quartz glass cube (3.8 cm on a side), with copper walls and heating coils surrounding the glass cell. Four of the copper walls contain small windows for optical access to the fuel. Heating is controlled by a PID controller (Eurotherm Model 818). The copper wall temperature is used as the input for the temperature controller. The fuel heat-up period is typically 20 minutes, and the setpoint temperature is achieved with no overshoot. The center temperature is held constant to within about 0.5% of the setpoint temperature. Detailed measurements with multiple thermocouples have shown that temperature gradients in this device are very small, with less

than 1% variation between temperatures at various locations in the liquid fuel (Klavetter et al., 1993).

Figure 12 displays the particle growth trends measured by PCS during 160°C heating of Jet A 91-POSF-2827 and Jet A 92-POSF-2922, respectively. The particle diameters shown are calculated from the autocorrelation signals using the CONTIN Laplace inversion routine. Essentially identical results were obtained with other available PCS data analysis algorithms (EXSAMP and MARLIN). The corresponding observed scattering intensities (normalized by the incident laser energy) as a function of exposure time are shown in Fig. 13. For both mean particle size and scattering intensity, the results for Jet A 92-POSF-2922 indicate a distinct induction time for particle formation. Once this "threshold" is achieved, however, the particle diameter increases rapidly. A concomitant increase in scattering intensity occurs until the mean particle diameter reaches approximately 500 nm. At that point, the scattering intensity appears to level off. Jet A 91-POSF-2827, on the other hand, exhibits facile production of small particles with essentially no induction time. The observed growth rate in particle size for this fuel is relatively slow compared to Jet A 92-POSF-2922. However, the scattering intensity data show that very large numbers of particles are formed. In fact, over most of the observed range in exposure times, the scattered light level from Jet A 91-POSF-2827 is nearly 10 times that of the other fuel. The rate of increase in the scattering intensity from Jet A 91-POSF-2827 diminishes with exposure time but continues to increase slowly at late times.

Figure 14 displays the particle growth trends measured by PCS during 150°C heating of all three fuels. In keeping with expectations of high thermal stability, the Jet A-1 fuel requires a very long induction time before particles become detectable; however, the particle growth rate is fairly rapid at late time. Jet A 92-POSF-2922 also exhibits a rapid growth rate as well as an induction time that is roughly half that of the Jet A-1. Once again, bulk particle formation can be detected at relatively short times in the case of Jet A 91-POSF-2827. Consistent with the PCS data acquired at 160°C, the growth rate in particle size appears to be relatively slow compared to the other two fuels. Figure 15 shows the normalized scattering intensity as a function of exposure time for the 150°C tests. As in the 160°C data, the scattering intensity for Jet A 92-POSF-2922 appears to level off as the mean particle diameter approaches 500 nm. It is interesting that the scattering intensity for the Jet A-1 90-POSF-2747 also levels out and even declines slightly after heating for approximately 275 minutes (255 minutes at temperature), although the particle diameters continue to grow during this time (see Fig. 14). This phenomenon may arise from particle-size-dependent fluctuations in the Mie intensity parameters, agglomeration of particles to form fewer large-diameter constituents, particle settling, or a combination of these effects (O'Hern et al.,

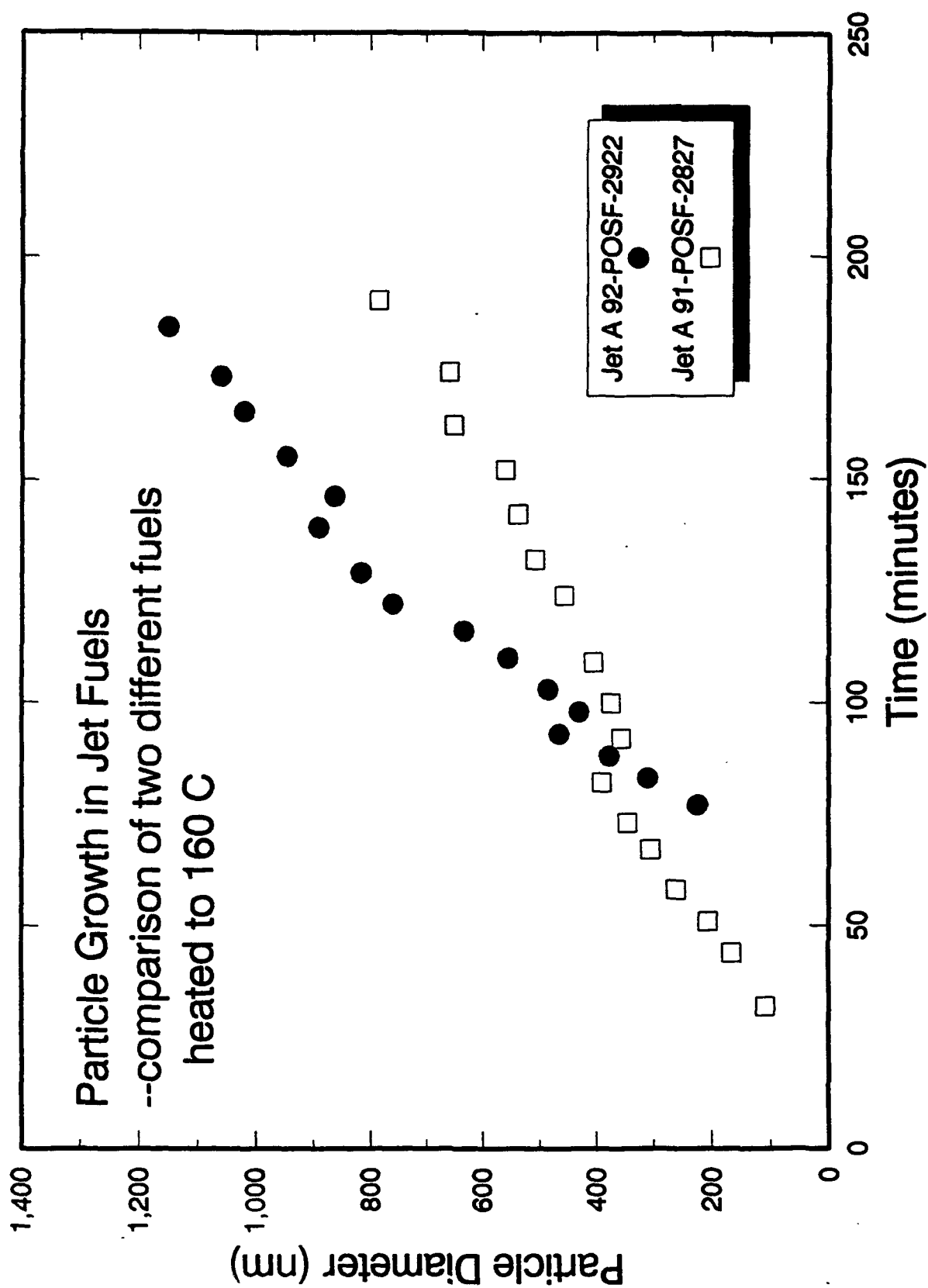


Figure 12. Particle growth rates measured by PCS for two fuels heated to 160°C.

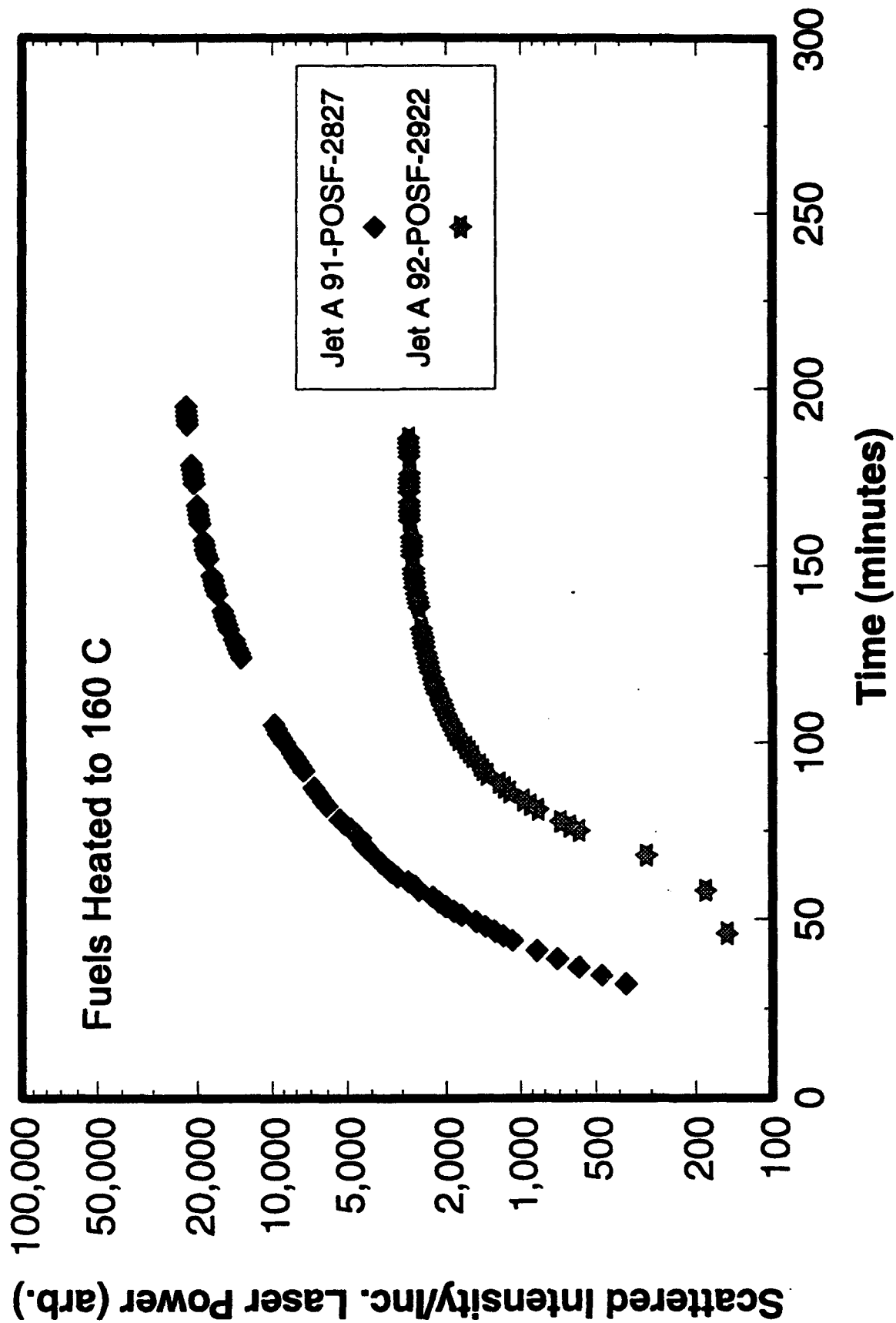


Figure 13. Normalized scattered light intensity for two fuels heated to 160°C.

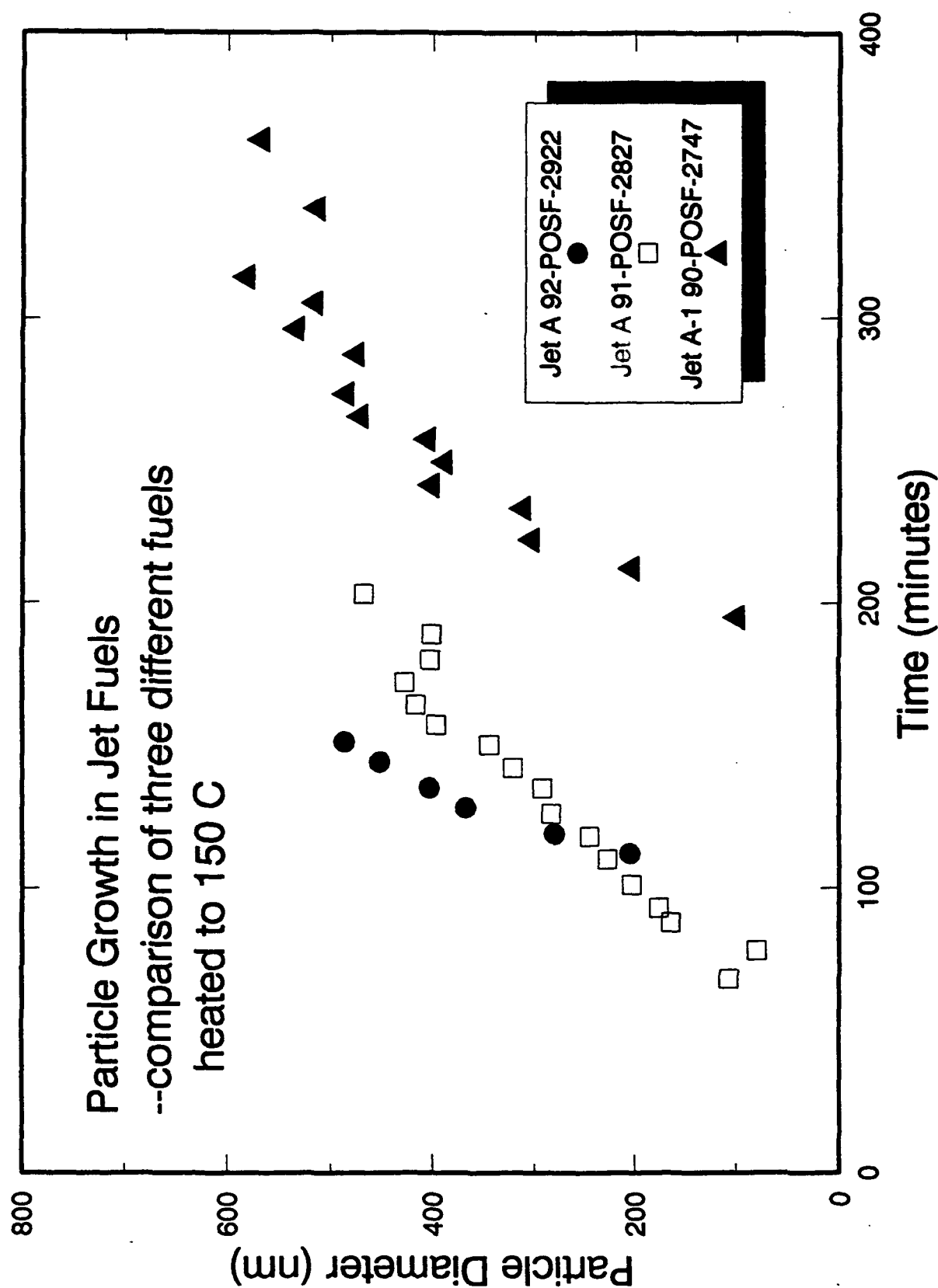


Figure 14. Particle growth rates measured by PCS for three fuels heated to 150°C.

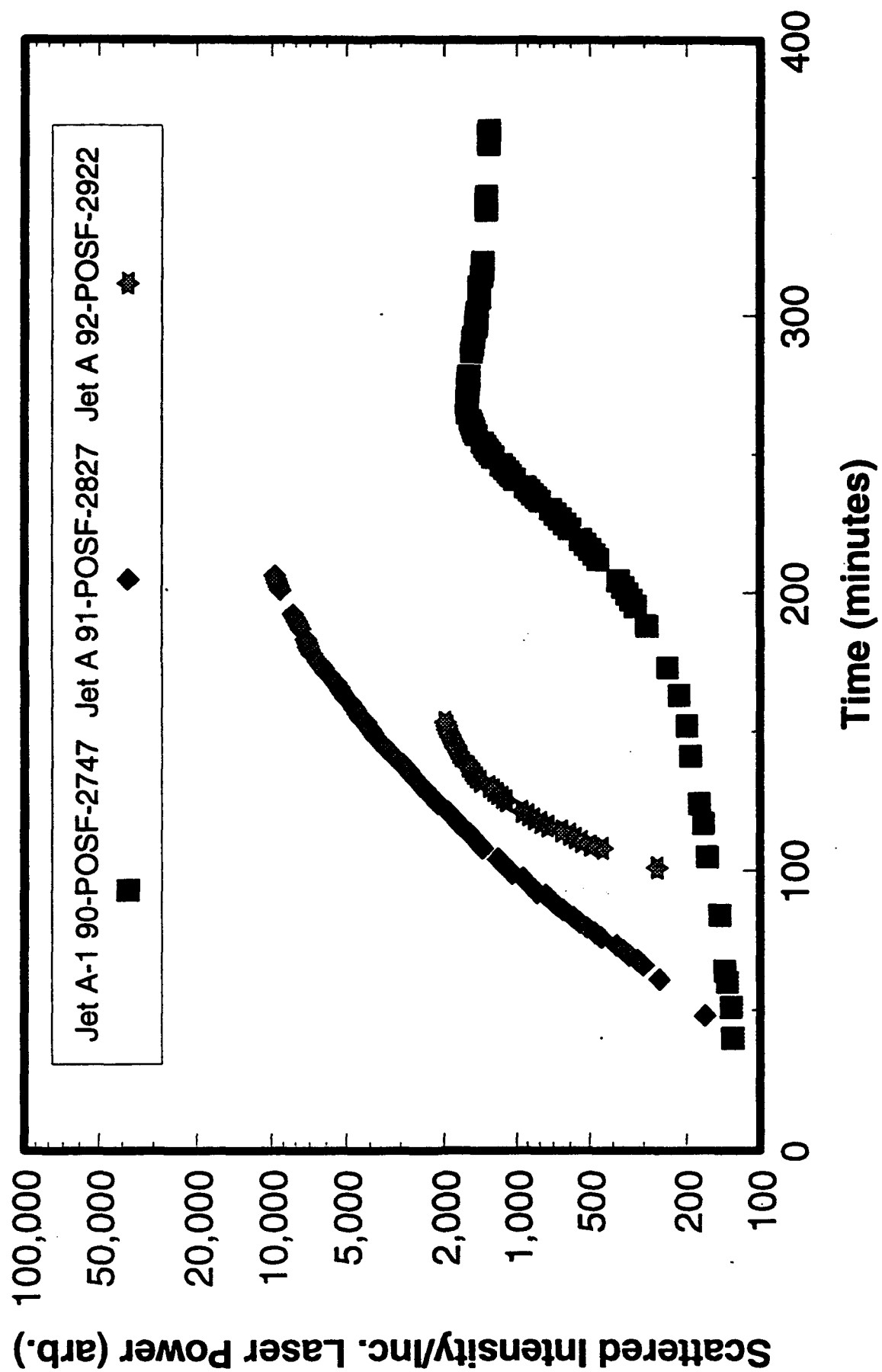


Figure 15. Normalized scattered light intensity for three fuels heated to 150°C.

1993). The facile particle formation in Jet A 91-POSF-2827 is clearly evident in the data shown in Fig. 15. At 200 minutes, the normalized scattering intensity is 30 times higher for this fuel than for Jet A-1 90-POSF-2747. PCS and scattering intensity data for Jet A 92-POSF-2922 and Jet A 91-POSF-2827 at 140°C are compared in Fig. 16 and Fig. 17, respectively. The results are consistent with those obtained at the other two temperatures.

The effects of stress temperature on the particle growth behavior of Jet A 91-POSF-2827 and Jet A 92-POSF-2922 are emphasized in Figs. 18 and 19, respectively. The latter figure also includes data acquired at 145°C, 134°C, and 125°C. In both cases, an increasingly longer exposure time is needed for particles to become detectable by PCS as the stress temperature is decreased. In addition, the particle growth rate can be seen to increase with increasing stress temperature. The apparent induction time for detectable particle formation is far more pronounced in the case of Jet A 92-POSF-2922, however. For this fuel, the observed induction time for substantial particle formation displays an Arrhenius-type dependence on temperature, as shown in Fig. 20. For temperatures in the range 134-160°C, the rate of increase in mean particle size exhibits a similar trend. This relationship is illustrated in Fig. 21. At 125°C, the particle growth rate appears to be significantly slower than the rate expected from an extrapolation of the higher temperature data.

In addition to determination of mean particle diameters, the PCS technique provides particle size distributions as well. Fig. 22 displays the evolution of size distributions observed during the real-time measurements in Jet A 92-POSF-2922 heated to 145°C. From tests performed thus far, fuel degradation typically results in a fairly narrow monomodal distribution of particle sizes, as long as temperature uniformity is maintained throughout the sample volume. Observed distribution widths (FWHM) appear to be 20-30% of the mean particle diameter. This value may be somewhat "inflated" by experimental factors; i.e., the need to limit sample times in conjunction with relatively rapid increases in particle diameter. Nevertheless, as discussed below, a reasonably accurate representation of the time-dependent particle-size distributions is valuable in estimation of the relative mass associated with particle formation in the bulk fluid.

Table 2 displays particle sizes measured post-test at room temperature. These data were recorded approximately 16-24 hours after the heating was terminated. The Jet A 91-POSF-2827 had the smallest particles present in the post-stressed case, and comparison of the tabulated values above with the stress test data (see Figs. 12, 14 and 16) shows that, for this fuel, the post-stressed mean particle diameter is essentially the same as the largest particle diameter achieved during the stress test, suggesting that the particle-growth mechanism essentially shuts off when the heating is terminated. On the other hand, the other fuel types displayed significantly larger particles post-test. For these fuels, the results

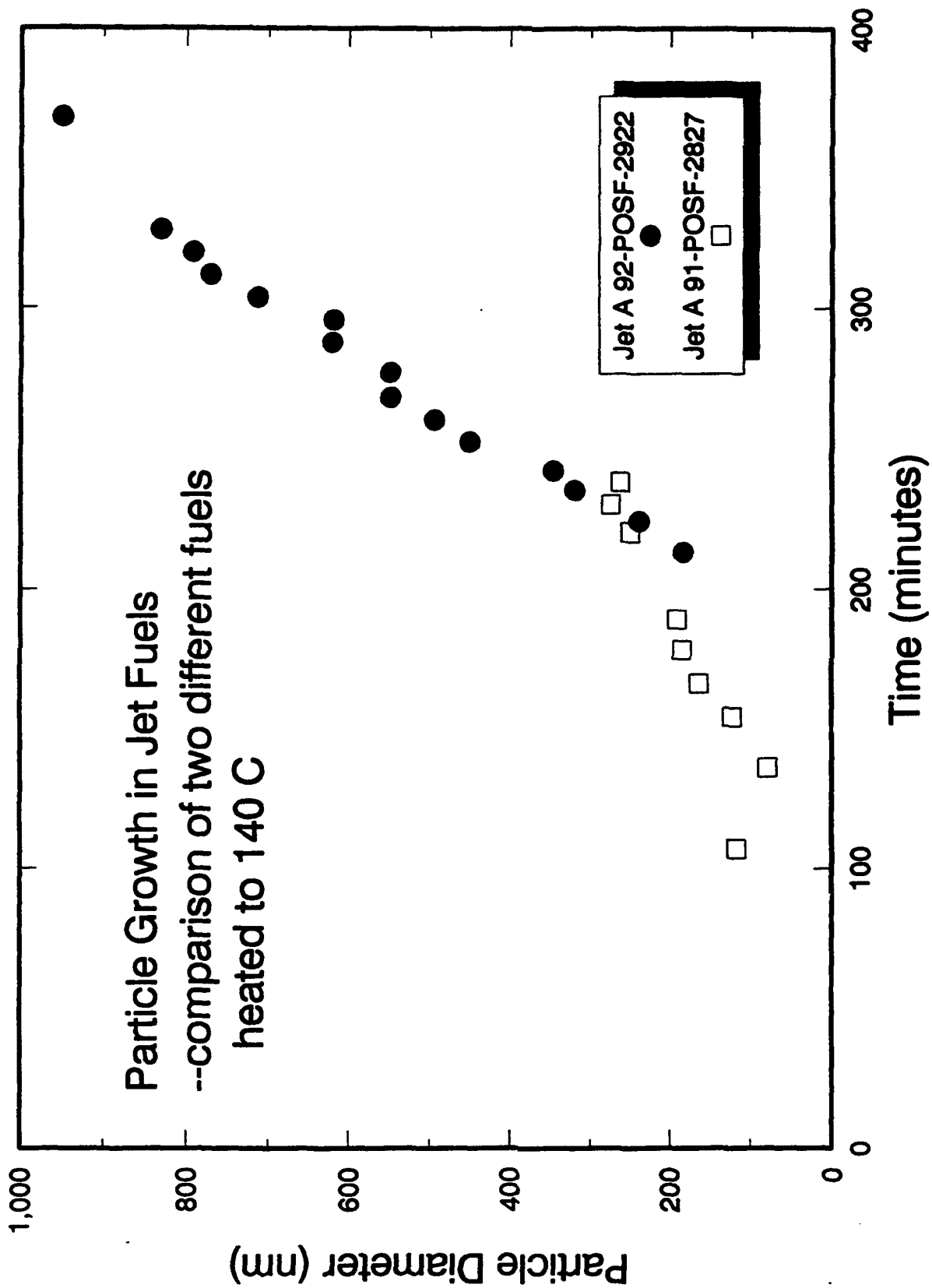


Figure 16. Particle growth rates measured by PCS for two fuels heated to 140°C.

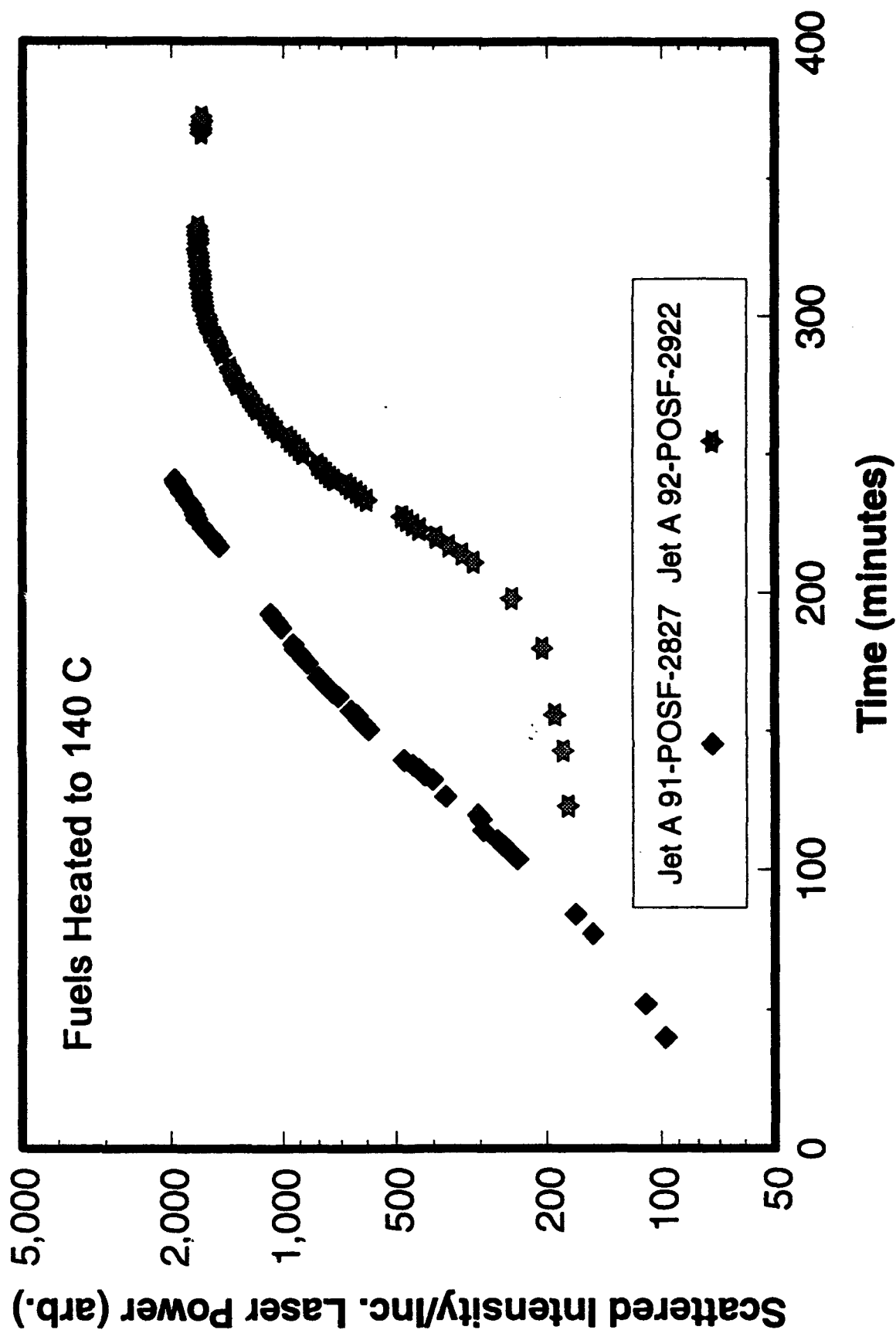


Figure 17. Normalized scattered light intensity for two fuels heated to 140°C.

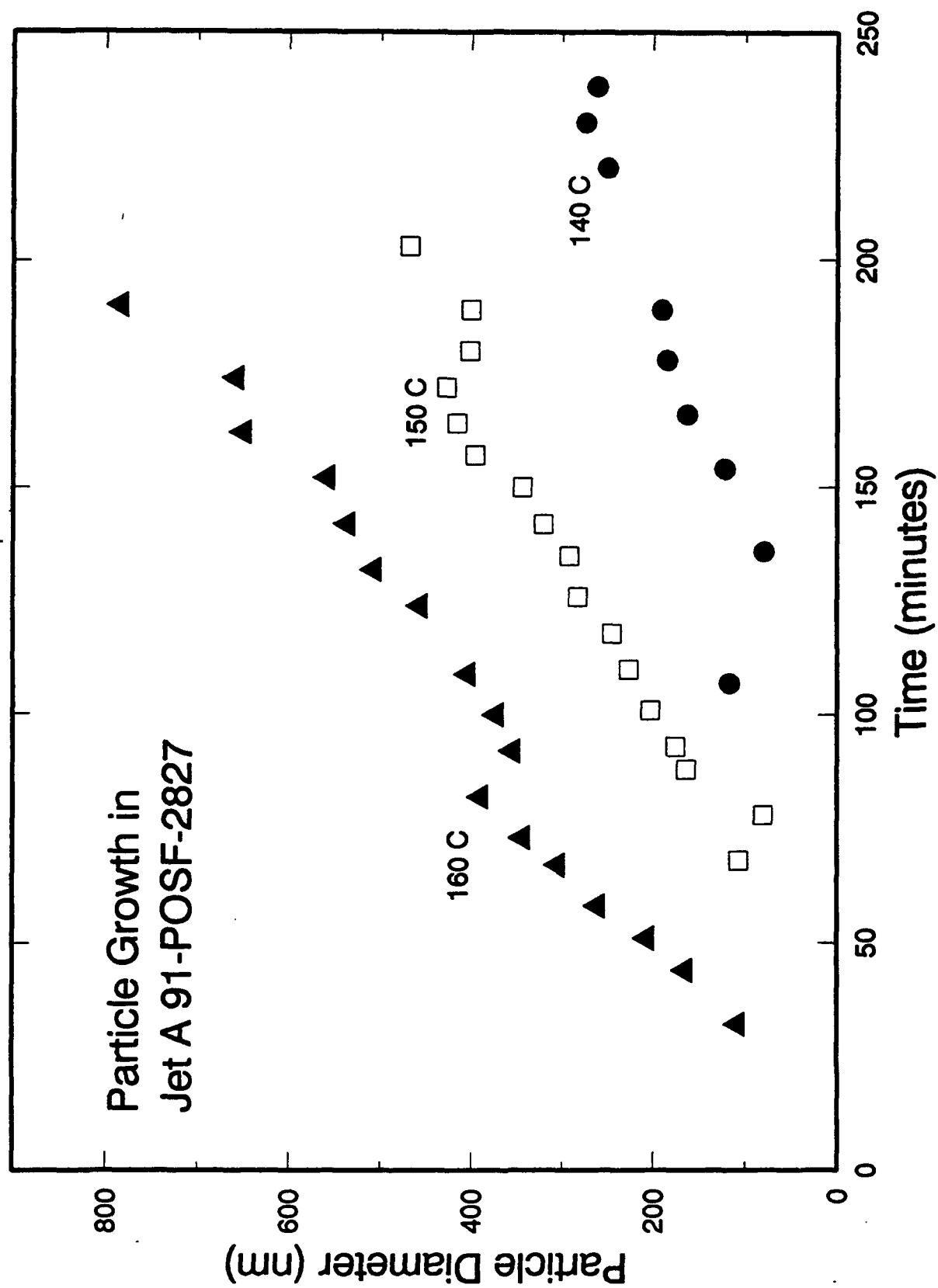


Figure 18. Particle diameters as a function of temperature and exposure time in Jet A 91-POSF-2827.

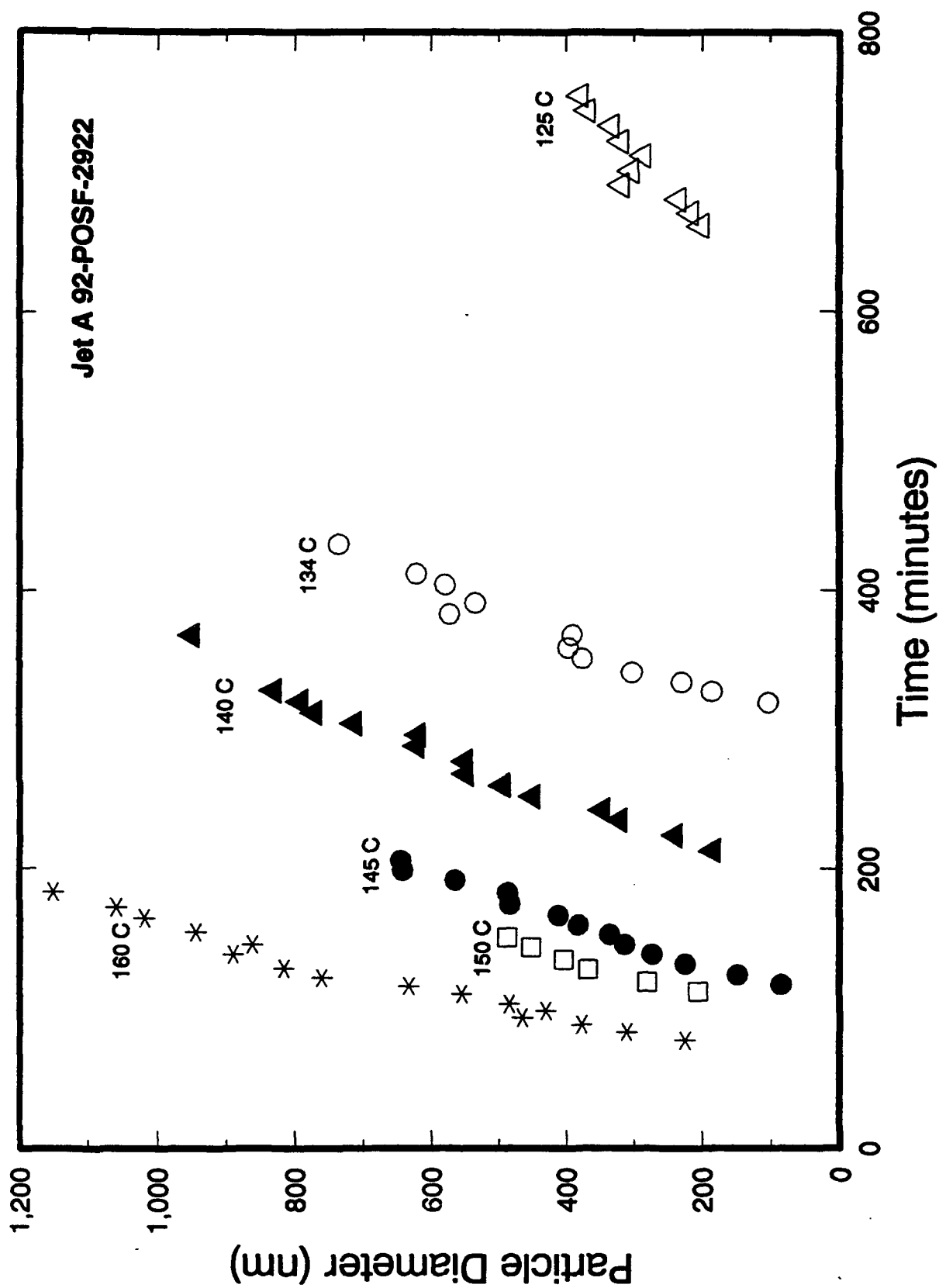


Figure 19. Particle diameters as a function of temperature and exposure time in Jet A 92-POSF-2922.

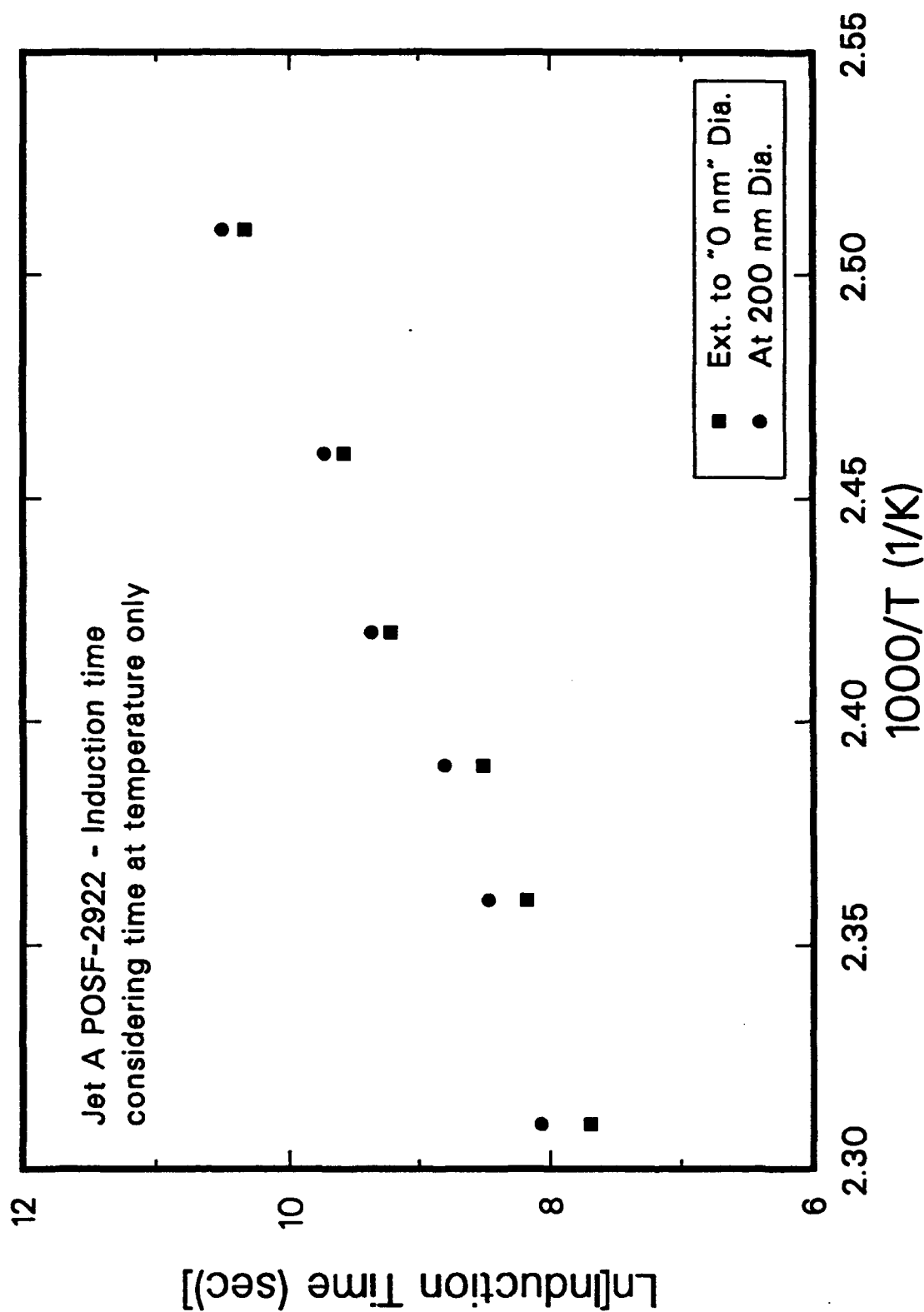


Figure 20. Induction times for detectable particle formation in Jet A 92-POSF-2922 as measured by PCS. Circles indicate the time required for mean particle diameter to reach 200 nm, squares the extrapolated time for particles to appear ("0 nm"--see Figure 19).

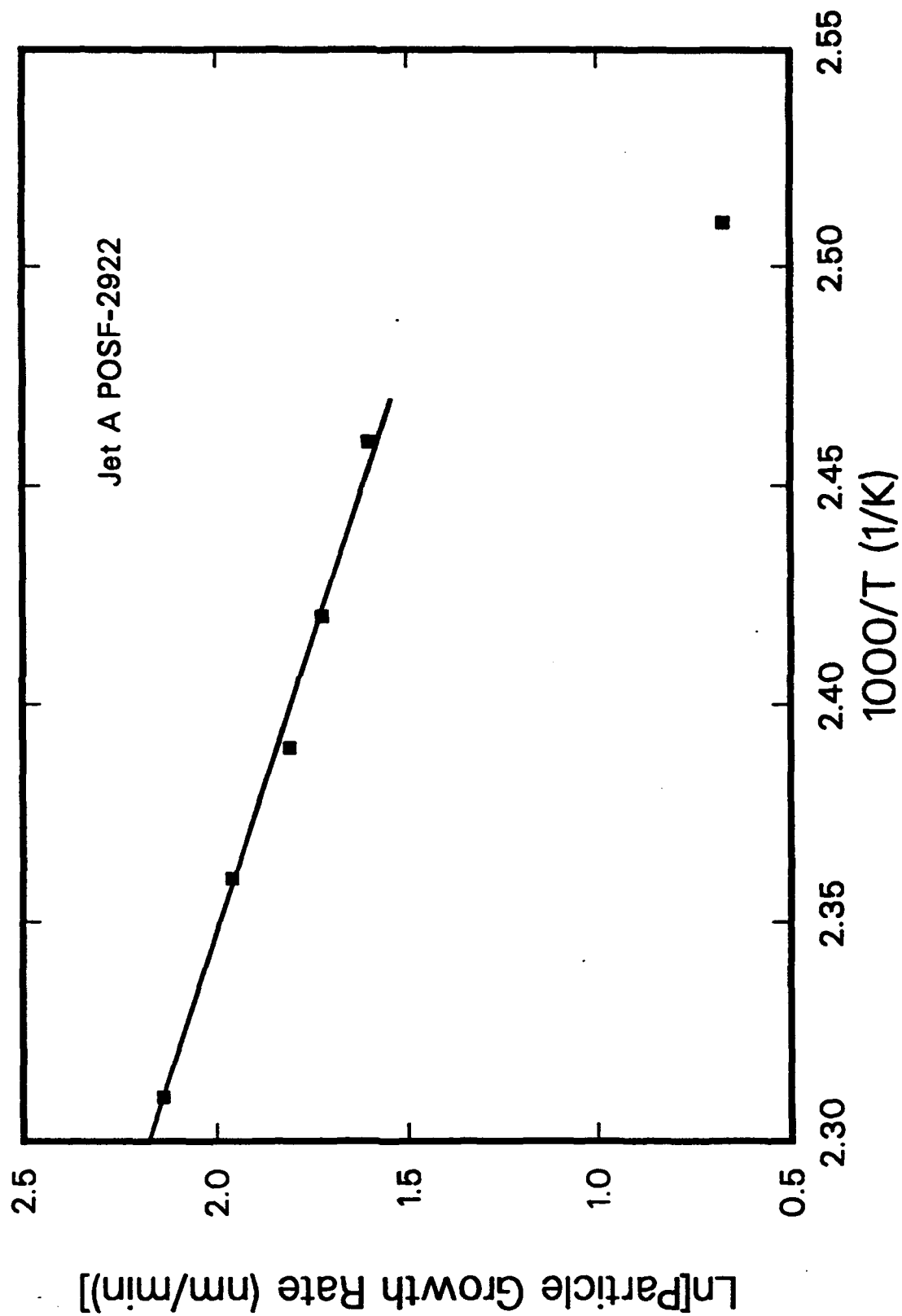


Figure 21. Arrhenius-type plot of PCS-measured particle growth rate in Jet A 92-POSF-2922.

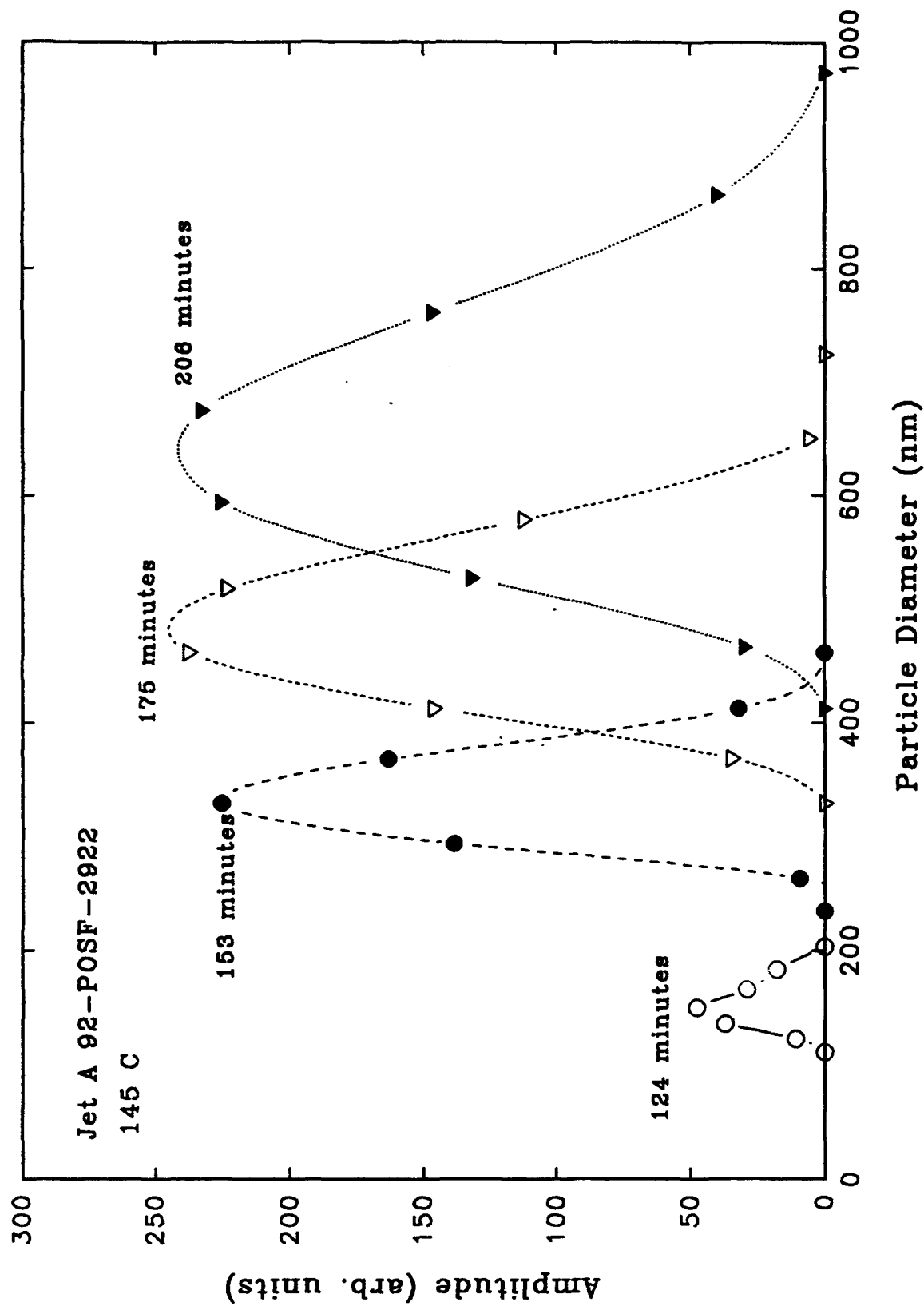


Figure 22. Real-time measurements of particle size distributions during 145°C heating of Jet A 92-POSF-2922.

indicate that particle growth continues after heating is terminated, as the tabulated diameters below are generally much larger than the final diameter achieved during stressing.

Table 2: Particle Sizes in Post-Stressed Fuels.

| Fuel | Stress Temperature | | |
|----------------------|--------------------|---------|---------|
| | 140°C | 150°C | 160°C |
| Jet A-1 90-POSF-2747 | ----- | 856 nm | 1150 nm |
| Jet A 91-POSF-2827 | 340 nm | 454 nm | 797 nm |
| Jet A 92-POSF-2922 | 1370 nm | 1400 nm | 1460 nm |

The visual appearance of the post-stressed fuels was generally consistent with the PCS and scattered light intensity results. Increased stress temperature produced more discoloration for all three fuels. The Jet A 92-POSF-2922 samples were significantly more discolored (deeper yellow) than the Jet A-1 specimens for both stress temperatures. It is interesting that relatively minor discoloration was observed in the post-test Jet A 91-POSF-2827 fuel; however, these samples exhibited a distinctly "cloudy" appearance due to the very large number of suspended particles.

The present comparison of these aviation fuels is interesting in light of earlier QCM results on the two Jet A fuels (O'Hern et al., 1993). The QCM tests showed that, for a given stress temperature, Jet A 92-POSF-2922 formed solids at a significantly higher deposition rate than Jet A 91-POSF-2827 under conditions of generous oxygen availability. This observation is in apparent contrast to the facile particle formation seen in the latter fuel under oxygen-lean conditions, as described above. However, tests showing the effect of oxygen availability on both solids deposition (as measured by the QCM system) and bulk particle formation (as determined by PCS) also pertain to the present results. Figure 23 shows PCS data from thermal stressing of Jet A 92-POSF-2922 fuel at 150°C. In one experiment, the fuel was subjected to the usual oxygen sparge prior to stressing; in the other experiment, oxygen was also continuously bubbled through the fuel during exposure to the elevated temperature. The greater availability of oxygen resulted in a substantially lower rate of increase in the mean particle diameter. As a result, for exposure times longer than 110 minutes, significantly larger particles were observed under oxygen-lean conditions. In contrast, a deficiency of oxygen dramatically decreases the solid deposition rate (O'Hern et al., 1993). The complex interplay of bulk particle formation versus solid deposition under different conditions of oxygen availability strongly indicates the need for integrated

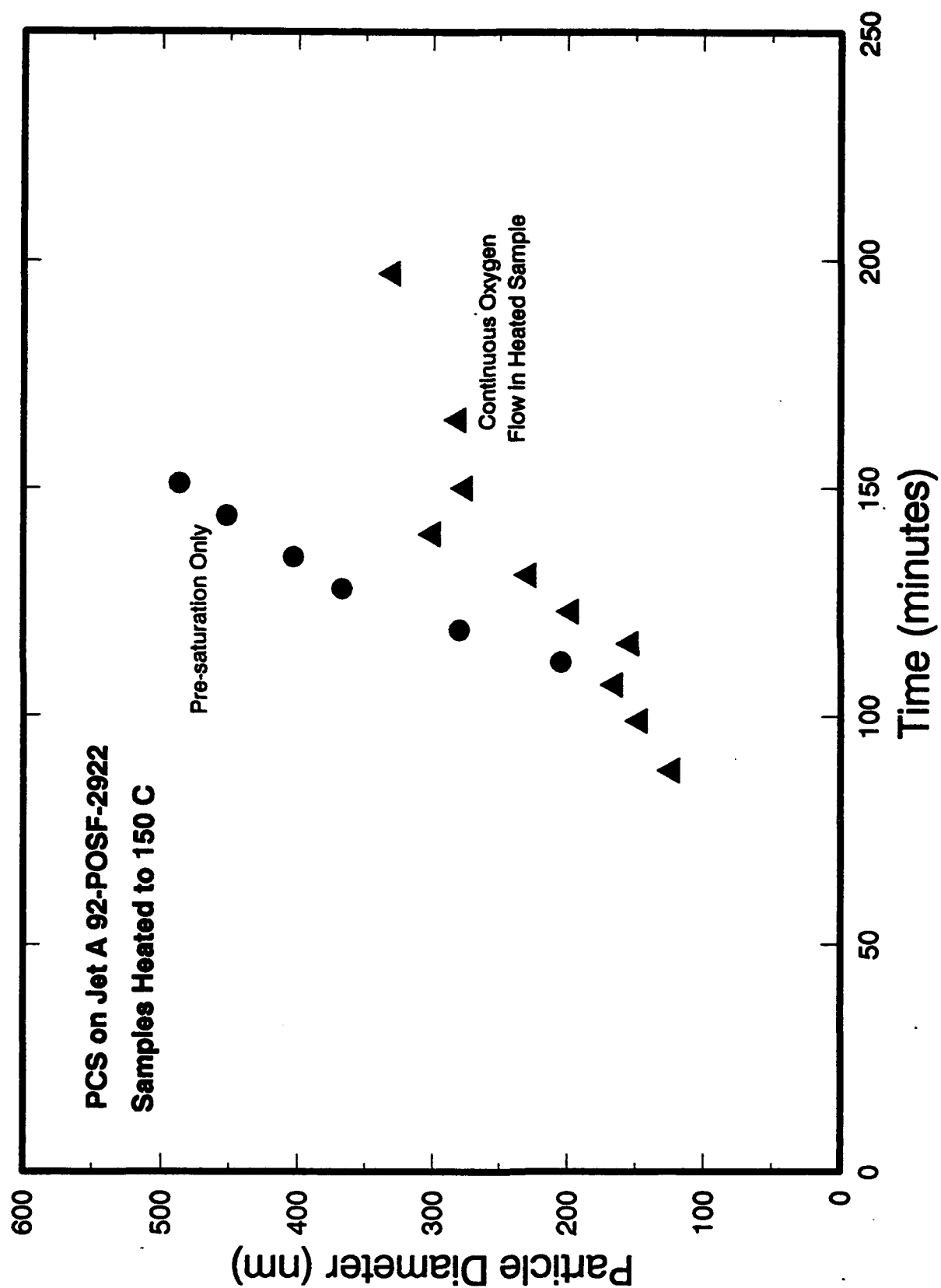


Figure 23. Effect of oxygen saturation on PCS-measured particle growth rate in Jet A 92-POSF-2922 heated to 150°C.

PCS/QCM experiments on the various fuels. Design and assembly of an experimental apparatus incorporating both techniques remain high priority items and preliminary attempts to integrate these diagnostic methods will be described below.

2.2.3 Diffusion Coefficients

Table 3 presents diffusion coefficient data for the three aviation fuels. The diffusion coefficients fall in the 2×10^{-7} to 2×10^{-8} cm²/s range. Although PCS measures the diffusion coefficient D directly, then uses it to calculate the particle diameter, our data file format does not list D . Therefore, the diffusion coefficients listed in the data table were calculated from the recorded mean particle diameters using the Stokes-Einstein equation:

$$D = \frac{k_B T}{3 \pi \mu d_p} \quad (10)$$

where k_B is the Boltzmann constant, T is the absolute temperature, μ is the liquid absolute viscosity, and d_p is the mean particle diameter. The Boltzmann constant is $k_B = 1.38 \times 10^{-23}$ J/K. The exact viscosity values for all fuels are unknown; the ones listed on the table and used here were extrapolated from available data and are assumed identical for the three fuels. The particle diameter values listed in Table 3 are mean values measured using the CONTIN Laplace inversion routine. The particle diameters determined by examining the autocorrelation function with other routines (e.g., CORAN (cumulants), MARLIN (exponential fitting), and EXSAMP (Laplace inversion)) agree to within about 10%. As mentioned previously, the CONTIN routine yields a mean diameter and a spread, which is typically on the order of ± 10 -15%, so there will be an equivalent distribution of diffusion coefficients

Comparison of the PCS and QCM data indicates that the particles depositing on surfaces may be smaller than those that are measured by PCS in the bulk fuel, since the QCM-measured deposition rates correspond to a deposit with a thickness approximately the same as one PCS-measured particle diameter. Therefore, the diffusion coefficients given here may be considered as minimum values.

Table 3: Particle Diameter and Diffusion Coefficient for Various Stress Temperatures

| Fuel Type | T(°C) | μ (cP) | Time at Temp. (min) | Mean Dia. (nm) | Mean Diffusion Coefficient D (cm ² /s) |
|------------|-------|------------|---------------------|----------------|---|
| Jet A 2922 | 125 | 0.332 | 661 | 201 | 8.73×10^{-8} |
| Jet A 2922 | 125 | 0.332 | 670 | 216 | 8.12×10^{-8} |
| Jet A 2922 | 125 | 0.332 | 680 | 234 | 7.50×10^{-8} |
| Jet A 2922 | 125 | 0.332 | 690 | 318 | 5.52×10^{-8} |
| Jet A 2922 | 125 | 0.332 | 700 | 303 | 5.79×10^{-8} |
| Jet A 2922 | 125 | 0.332 | 711 | 285 | 6.16×10^{-8} |
| Jet A 2922 | 125 | 0.332 | 721 | 318 | 5.52×10^{-8} |
| Jet A 2922 | 125 | 0.332 | 732 | 332 | 5.29×10^{-8} |
| Jet A 2922 | 125 | 0.332 | 743 | 367 | 4.78×10^{-8} |
| Jet A 2922 | 125 | 0.332 | 754 | 378 | 4.64×10^{-8} |
| | | | | | |
| Jet A 2922 | 135 | 0.298 | 319 | 102 | 1.96×10^{-7} |
| Jet A 2922 | 135 | 0.298 | 327 | 185 | 1.08×10^{-7} |
| Jet A 2922 | 135 | 0.298 | 334 | 229 | 8.75×10^{-8} |
| Jet A 2922 | 135 | 0.298 | 341 | 302 | 6.64×10^{-8} |
| Jet A 2922 | 135 | 0.298 | 351 | 375 | 5.34×10^{-8} |
| Jet A 2922 | 135 | 0.298 | 359 | 396 | 5.06×10^{-8} |
| Jet A 2922 | 135 | 0.298 | 368 | 390 | 5.14×10^{-8} |
| Jet A 2922 | 135 | 0.298 | 383 | 572 | 3.50×10^{-8} |
| Jet A 2922 | 135 | 0.298 | 391 | 534 | 3.75×10^{-8} |
| Jet A 2922 | 135 | 0.298 | 404 | 579 | 3.46×10^{-8} |
| Jet A 2922 | 135 | 0.298 | 412 | 622 | 3.22×10^{-8} |
| Jet A 2922 | 135 | 0.298 | 433 | 736 | 2.72×10^{-8} |
| | | | | | |
| Jet A 2922 | 140 | 0.283 | 213 | 184 | 1.16×10^{-7} |

Table 3: Particle Diameter and Diffusion Coefficient for Various Stress Temperatures (Cont'd)

| Fuel Type | T(°C) | μ (cP) | Time at Temp. (min) | Mean Dia. (nm) | Mean Diffusion Coefficient D (cm ² /s) |
|------------|-------|------------|---------------------|----------------|---|
| Jet A 2922 | 140 | 0.283 | 224 | 239 | 8.94x10 ⁻⁸ |
| Jet A 2922 | 140 | 0.283 | 235 | 320 | 6.68x10 ⁻⁸ |
| Jet A 2922 | 140 | 0.283 | 242 | 346 | 6.17x10 ⁻⁸ |
| Jet A 2922 | 140 | 0.283 | 252 | 450 | 4.75x10 ⁻⁸ |
| Jet A 2922 | 140 | 0.283 | 260 | 494 | 4.32x10 ⁻⁸ |
| Jet A 2922 | 140 | 0.283 | 268 | 548 | 3.90x10 ⁻⁸ |
| Jet A 2922 | 140 | 0.283 | 277 | 549 | 3.89x10 ⁻⁸ |
| Jet A 2922 | 140 | 0.283 | 288 | 621 | 3.44x10 ⁻⁸ |
| Jet A 2922 | 140 | 0.283 | 296 | 619 | 3.45x10 ⁻⁸ |
| Jet A 2922 | 140 | 0.283 | 304 | 713 | 3.00x10 ⁻⁸ |
| Jet A 2922 | 140 | 0.283 | 312 | 771 | 2.77x10 ⁻⁸ |
| Jet A 2922 | 140 | 0.283 | 320 | 792 | 2.70x10 ⁻⁸ |
| Jet A 2922 | 140 | 0.283 | 328 | 831 | 2.57x10 ⁻⁸ |
| Jet A 2922 | 140 | 0.283 | 368 | 950 | 2.25x10 ⁻⁸ |
| | | | | | |
| Jet A 2922 | 150 | 0.255 | 88 | 123 | 1.97x10 ⁻⁷ |
| Jet A 2922 | 150 | 0.255 | 99 | 147 | 1.65x10 ⁻⁷ |
| Jet A 2922 | 150 | 0.255 | 107 | 165 | 1.47x10 ⁻⁷ |
| Jet A 2922 | 150 | 0.255 | 116 | 153 | 1.59x10 ⁻⁷ |
| Jet A 2922 | 150 | 0.255 | 123 | 197 | 1.23x10 ⁻⁷ |
| Jet A 2922 | 150 | 0.255 | 131 | 228 | 1.06x10 ⁻⁷ |
| Jet A 2922 | 150 | 0.255 | 140 | 300 | 8.10x10 ⁻⁷ |
| Jet A 2922 | 150 | 0.255 | 150 | 276 | 8.80x10 ⁻⁷ |
| Jet A 2922 | 150 | 0.255 | 165 | 281 | 8.64x10 ⁻⁷ |
| Jet A 2922 | 150 | 0.255 | 197 | 330 | 7.36x10 ⁻⁷ |
| | | | | | |

Table 3: Particle Diameter and Diffusion Coefficient for Various Stress Temperatures (Cont'd)

| Fuel Type | T(°C) | μ (cP) | Time at Temp. (min) | Mean Dia. (nm) | Mean Diffusion Coefficient D (cm ² /s) |
|--------------|-------|------------|---------------------|----------------|---|
| Jet A 2922 | 160 | 0.231 | 77 | 224 | 1.22×10^{-7} |
| Jet A 2922 | 160 | 0.231 | 83 | 310 | 8.85×10^{-8} |
| Jet A 2922 | 160 | 0.231 | 93 | 465 | 5.90×10^{-8} |
| Jet A 2922 | 160 | 0.231 | 98 | 430 | 6.38×10^{-8} |
| Jet A 2922 | 160 | 0.231 | 103 | 484 | 5.67×10^{-8} |
| Jet A 2922 | 160 | 0.231 | 110 | 554 | 4.95×10^{-8} |
| Jet A 2922 | 160 | 0.231 | 116 | 633 | 4.33×10^{-8} |
| Jet A 2922 | 160 | 0.231 | 122 | 760 | 3.61×10^{-8} |
| Jet A 2922 | 160 | 0.231 | 129 | 816 | 3.36×10^{-8} |
| Jet A 2922 | 160 | 0.231 | 139 | 890 | 3.08×10^{-8} |
| Jet A 2922 | 160 | 0.231 | 146 | 862 | 3.18×10^{-8} |
| Jet A 2922 | 160 | 0.231 | 155 | 945 | 2.90×10^{-8} |
| Jet A 2922 | 160 | 0.231 | 165 | 1019 | 2.69×10^{-8} |
| Jet A 2922 | 160 | 0.231 | 173 | 1059 | 2.59×10^{-8} |
| Jet A 2922 | 160 | 0.231 | 184 | 1150 | 2.39×10^{-8} |
| | | | | | |
| Jet A-1 2747 | 160 | 0.231 | 90 | 155 | 1.77×10^{-7} |
| Jet A-1 2747 | 160 | 0.231 | 110 | 220 | 1.25×10^{-7} |
| Jet A-1 2747 | 160 | 0.231 | 120 | 230 | 1.19×10^{-7} |
| Jet A-1 2747 | 160 | 0.231 | 145 | 255 | 1.08×10^{-7} |
| Jet A-1 2747 | 160 | 0.231 | 149 | 301 | 9.12×10^{-8} |
| Jet A-1 2747 | 160 | 0.231 | 165 | 280 | 9.80×10^{-8} |
| Jet A-1 2747 | 160 | 0.231 | 225 | 355 | 7.73×10^{-8} |
| Jet A-1 2747 | 160 | 0.231 | 245 | 405 | 6.78×10^{-8} |
| Jet A-1 2747 | 160 | 0.231 | 280 | 408 | 6.73×10^{-8} |

Table 3: Particle Diameter and Diffusion Coefficient for Various Stress Temperatures (Cont'd)

| Fuel Type | T(°C) | μ (cP) | Time at Temp. (min) | Mean Dia. (nm) | Mean Diffusion Coefficient D (cm ² /s) |
|--------------|-------|------------|---------------------|----------------|---|
| Jet A-1 2747 | 150 | 0.255 | 175 | 99 | 2.45×10^{-7} |
| Jet A-1 2747 | 150 | 0.255 | 192 | 203 | 1.20×10^{-7} |
| Jet A-1 2747 | 150 | 0.255 | 202 | 303 | 8.01×10^{-8} |
| Jet A-1 2747 | 150 | 0.255 | 213 | 311 | 7.81×10^{-8} |
| Jet A-1 2747 | 150 | 0.255 | 221 | 401 | 6.06×10^{-8} |
| Jet A-1 2747 | 150 | 0.255 | 229 | 388 | 6.26×10^{-8} |
| Jet A-1 2747 | 150 | 0.255 | 237 | 405 | 600×10^{-8} |
| Jet A-1 2747 | 150 | 0.255 | 245 | 471 | 5.15×10^{-8} |
| Jet A-1 2747 | 150 | 0.255 | 253 | 485 | 5.01×10^{-8} |
| Jet A-1 2747 | 150 | 0.255 | 267 | 475 | 5.11×10^{-8} |
| Jet A-1 2747 | 150 | 0.255 | 276 | 534 | 4.55×10^{-8} |
| Jet A-1 2747 | 150 | 0.255 | 285 | 516 | 4.71×10^{-8} |
| Jet A-1 2747 | 150 | 0.255 | 294 | 582 | 4.17×10^{-8} |
| Jet A-1 2747 | 150 | 0.255 | 318 | 514 | 4.72×10^{-8} |
| Jet A-1 2747 | 150 | 0.255 | 342 | 568 | 4.28×10^{-8} |
| | | | | | |
| Jet A 2827 | 150 | 0.255 | 48 | 107 | 2.27×10^{-7} |
| Jet A 2827 | 150 | 0.255 | 58 | 80 | 3.04×10^{-7} |
| Jet A 2827 | 150 | 0.255 | 68 | 164 | 1.48×10^{-7} |
| Jet A 2827 | 150 | 0.255 | 73 | 176 | 1.38×10^{-7} |
| Jet A 2827 | 150 | 0.255 | 81 | 203 | 1.20×10^{-7} |
| Jet A 2827 | 150 | 0.255 | 90 | 227 | 1.07×10^{-7} |
| Jet A 2827 | 150 | 0.255 | 98 | 245 | 9.91×10^{-7} |
| Jet A 2827 | 150 | 0.255 | 106 | 283 | 8.58×10^{-7} |
| Jet A 2827 | 150 | 0.255 | 115 | 292 | 8.32×10^{-8} |

Table 3: Particle Diameter and Diffusion Coefficient for Various Stress Temperatures (Cont'd)

| Fuel Type | T(°C) | μ (cP) | Time at Temp. (min) | Mean Dia. (nm) | Mean Diffusion Coefficient D (cm ² /s) |
|------------|-------|------------|---------------------|----------------|---|
| Jet A 2827 | 150 | 0.255 | 122 | 321 | 7.56×10^{-8} |
| Jet A 2827 | 150 | 0.255 | 230 | 344 | 7.06×10^{-8} |
| Jet A 2827 | 150 | 0.255 | 137 | 396 | 6.13×10^{-8} |
| Jet A 2827 | 150 | 0.255 | 144 | 416 | 5.84×10^{-8} |
| Jet A 2827 | 150 | 0.255 | 152 | 427 | 5.69×10^{-8} |
| Jet A 2827 | 150 | 0.255 | 160 | 402 | 6.04×10^{-8} |
| Jet A 2827 | 150 | 0.255 | 169 | 401 | 6.06×10^{-8} |
| Jet A 2827 | 150 | 0.255 | 183 | 468 | 5.19×10^{-8} |
| | | | | | |
| Jet A 2827 | 160 | 0.231 | 12 | 108 | 2.54×10^{-7} |
| Jet A 2827 | 160 | 0.231 | 24 | 165 | 1.66×10^{-7} |
| Jet A 2827 | 160 | 0.231 | 31 | 207 | 1.32×10^{-7} |
| Jet A 2827 | 160 | 0.231 | 38 | 261 | 1.05×10^{-7} |
| Jet A 2827 | 160 | 0.231 | 47 | 305 | 9.00×10^{-8} |
| Jet A 2827 | 160 | 0.231 | 53 | 344 | 7.98×10^{-8} |
| Jet A 2827 | 160 | 0.231 | 62 | 390 | 7.04×10^{-8} |
| Jet A 2827 | 160 | 0.231 | 72 | 355 | 7.73×10^{-8} |
| Jet A 2827 | 160 | 0.231 | 80 | 373 | 7.36×10^{-8} |
| Jet A 2827 | 160 | 0.231 | 104 | 456 | 6.02×10^{-8} |
| Jet A 2827 | 160 | 0.231 | 112 | 507 | 5.41×10^{-8} |
| Jet A 2827 | 160 | 0.231 | 122 | 536 | 5.12×10^{-8} |
| Jet A 2827 | 160 | 0.231 | 132 | 558 | 4.92×10^{-8} |
| Jet A 2827 | 160 | 0.231 | 142 | 650 | 4.22×10^{-8} |
| Jet A 2827 | 160 | 0.231 | 154 | 658 | 4.17×10^{-8} |
| Jet A 2827 | 160 | 0.231 | 170 | 784 | 3.50×10^{-8} |

2.2.4 Refractive Index Measurements

The fuel refractive index, n , is needed for quantitative analysis of PCS data. This parameter is required in the calculation of the scattering wave vector, which in turn permits determination of the translational diffusion coefficient from the decay rate of the observed autocorrelation function (Trott et al., 1992). An important concern is the possible effect of thermal stressing on this parameter. We have used a Bausch & Lomb ABBE-3L Refractometer to determine n for fuel samples before and after thermal stressing. For unstressed Jet A 92-POSF-2922, n was determined to be 1.4473. Post-test examination of this fuel after heating to 160°C demonstrated that n was practically unchanged ($n=1.4478$). This result indicates that any modification to n due to fuel chemistry or particle formation is probably minor compared to the effect of temperature on this parameter (also relatively small). We have yet to incorporate the temperature-induced change in n into analysis of real-time PCS data since the exact values have not been determined for the various aviation fuels. We are evaluating methods for modifying the sampling system of the refractometer to permit tests at temperatures up to 200°C

2.2.5 Integration of PCS and QCM Techniques

In an initial effort to incorporate the QCM diagnostic technique into the PCS test assembly, fresh QCM wafers were included in fuel samples that were heated in the optical quartz glass cube and examined with the usual dynamic light scattering and scattering intensity data collection methods. After thermal stressing of the fuel, the QCM wafers were dried and evaluated for mass deposition. Two tests were carried out in this manner: (1) Jet A-1 90-POSF-2747 heated to 160°C and maintained at temperature for two hours, and (2) Jet A 92-POSF-2922 heated to 160°C for a similar length of time. Values for total mass deposition during these tests were found to be relatively low; i.e., 2.18 $\mu\text{g}/\text{cm}^2$ and 3.84 $\mu\text{g}/\text{cm}^2$, respectively.

Recently, we have conducted joint real-time PCS/QCM tests with the QCM driven by the "second generation" oscillator circuit and data acquisition system described in Klavetter et al., 1993. For these tests, conducting leads were attached to the QCM wafer using a high-temperature, Ag-filled polyimide adhesive. These leads were required to position the QCM out of the path of the illuminating laser (for PCS) and still permit the use of a lid on the quartz glass cube (to retard fuel evaporation). Results of these preliminary experiments are shown in Fig. 24 and Fig. 25. In the test with Jet A 91-POSF-2827 heated to 150°C (cf. Fig. 24), QCM data acquisition was started 20 minutes after heating commenced. The mass accumulation data exhibited a monotonic "negative" excursion initially, likely due to a slight

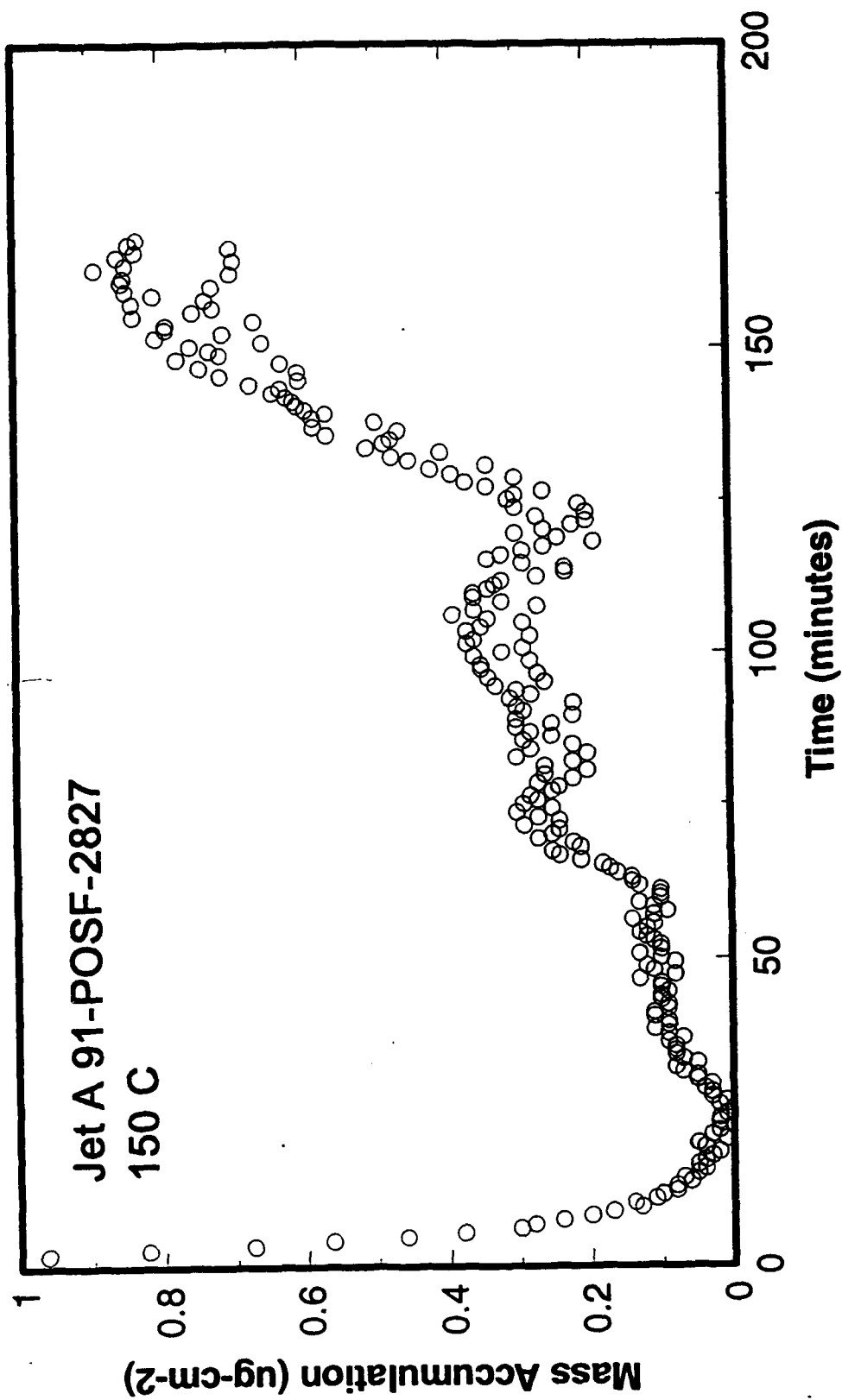


Figure 24. QCM mass deposition data in Jet A 91-POSF-2827 heated to 150°C. Test performed in PCS experimental set-up.

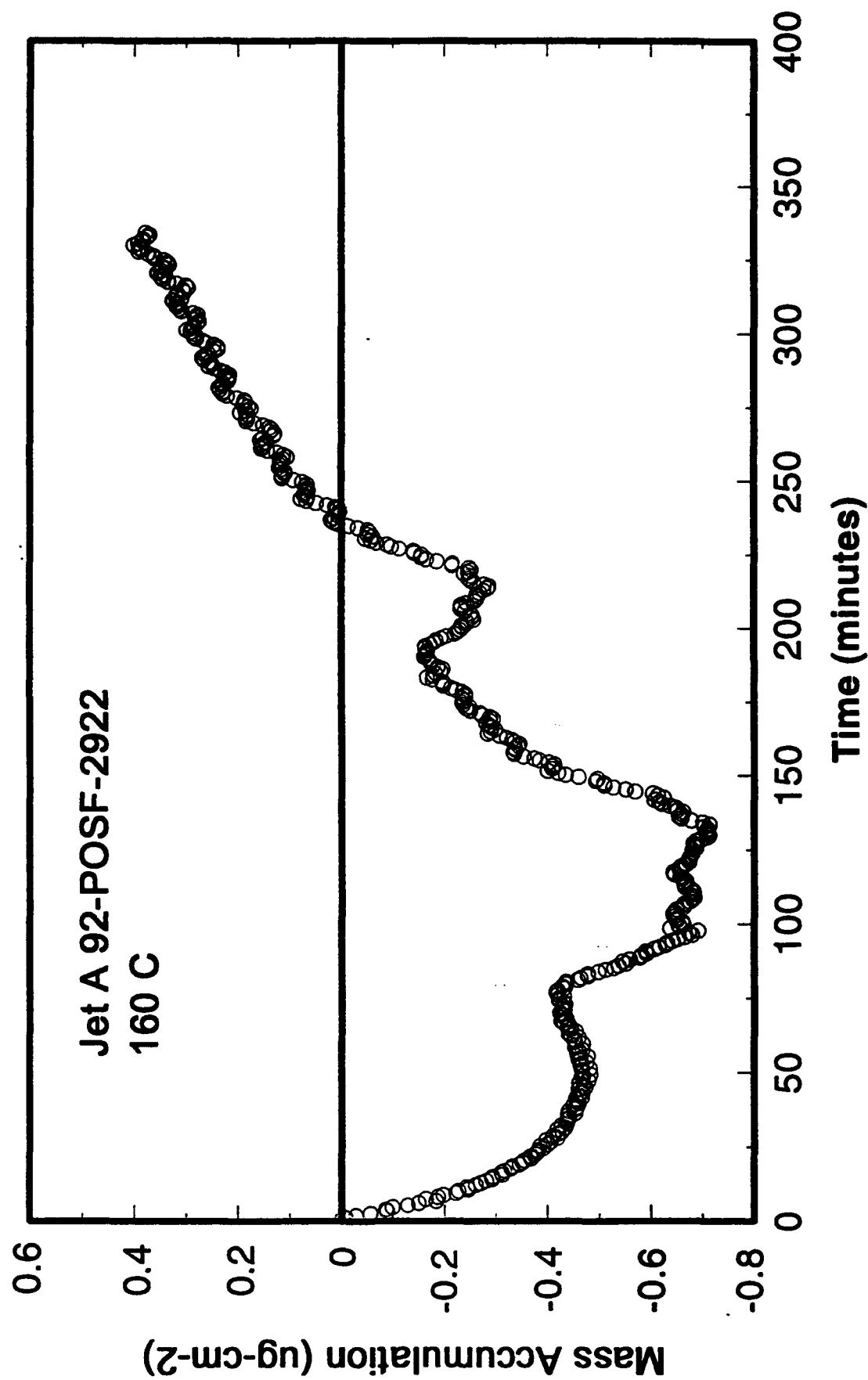


Figure 25. QCM mass deposition data in Jet A 92-POSF-2922 heated to 160°C. Test performed in PCS experimental set-up.

Increase in temperature in the cell at this early time. Subsequently, a roughly linear increase was observed for approximately 90 minutes. This portion of the data probably reflects actual mass deposition during this interval. Accordingly, the data have been offset to set "zero" mass accumulation at the onset of the linear increase. The mass deposition rate indicated by this data is extremely low; i.e., $\sim 0.25 \mu\text{g}/\text{cm}^2\text{-hr}$. Inconsistent data (reflected in substantial excursions in voltage) were obtained after this interval and the device failed to oscillate after approximately 3 hours of data collection. In contrast, the QCM used in the examination of Jet A 92-POSF-2922 at 160°C remained in oscillation throughout the entire 6-hour test (cf. Fig. 25). In this case, the observed trends in the mass accumulation data seem to reflect (as before) a very low rate of mass deposition coupled with variations due to small temperature fluctuations. If the linear portion of the data obtained near the end of the test is used to calculate the deposition rate, the value is once again near $0.25 \mu\text{g}/\text{cm}^2\text{-hr}$. A test was performed using the QCM-JFTS described in Section 2.1 on the same fuel at 160°C and with no overpressure to simulate the conditions in the integrated PCS-QCM test; stirring occurred in the QCM-JFTS test cell to facilitate temperature uniformity while no stirring occurred in the PCS tests. The QCM-JFTS test obtained a mass deposition rate of $0.15 \mu\text{g}/\text{cm}^2\text{-hr}$, comparable to that obtained with the integrated PCS-QCM test.

To date, multiple thermocouple measurements have not been made with a QCM wafer present in the quartz cell. It is possible that the wafer significantly perturbs the convective flows that are thought to contribute to temperature uniformity within this device. However, it should be noted that PCS data acquired during these tests are very consistent with results obtained in the absence of a QCM. Figure 26 shows particle diameter versus exposure time curves for three runs on Jet A 91-POSF-2827 at 150°C , two of which included QCMs. The three curves are essentially identical with respect to the onset of particle detection as well as the rate of increase in particle diameter.

Based on joint PCS/QCM tests conducted thus far, several observations can be made. First, the apparently low rate of mass deposition suggests that comparative runs with generous oxygen availability should be performed. Second, the degree of temperature uniformity in the test cell containing the QCM should be evaluated and optimized. Finally, a more reliable mount and electrical connection to the QCM need to be obtained. To address these concerns, a stainless steel pressure vessel (300 ml. capacity) similar to those in use with existing QCM test assemblies has been ordered from Parr Instrument Co. This vessel will provide the requisite optical access for PCS, a lid containing the QCM mounting clamp in common use (Klavetter et al., 1993), and the capacity to maintain overpressures of oxygen or

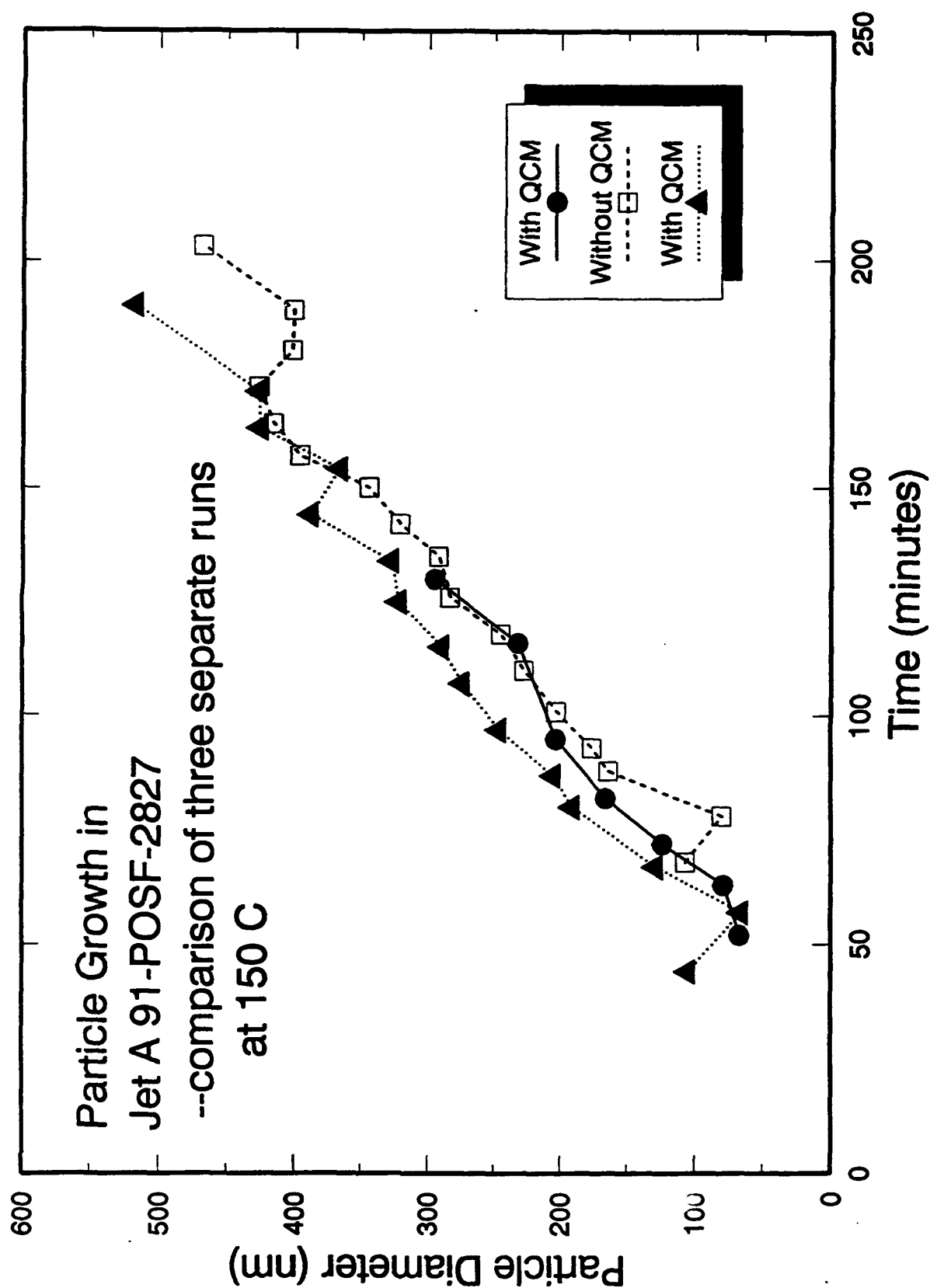


Figure 26. Particle growth rates measured by PCS in Jet A 91-POSF-2827. Comparison of three runs at 150°C (with and without QCM in cell).

other gases during thermal stress tests. With these system improvements, it is anticipated that quantitative comparisons of PCS and QCM data can be made.

2.2.6 Relative Mass Calculations

Although mean particle diameters and particle size distributions are useful in evaluating particle formation mechanisms in the bulk liquid, a more fundamental quantity of interest is the mass growth associated with particle generation. This information is particularly valuable in connection with concurrent mass deposition data (e.g., as acquired by a QCM). To provide an estimate of mass growth in particles, we have calculated the increase in relative mass from Mie intensity parameters (determined by the Mie scattering algorithm "CALLBH" described in Bohren and Huffman, 1983) in combination with observed scattering intensities versus time. These computations utilize both the mean particle diameter and the particle size distributions determined by PCS in arriving at a relative particle number density associated with a given scattering intensity. Results for Jet A 91-POSF-2827 heated to 160°C are shown in Fig.27. For these calculations, the refractive index of the scattering particles was assumed to be ~10% higher than the liquid refractive index (Bolshakov, 1974) and the mass density of the particles was assumed to be independent of the particle diameter. Despite uncertainties due to these assumptions as well as the analysis of integrated scattering intensities in terms of discrete particle size distributions, it is clear that mass growth occurs in two regimes in this system. A rapid increase in mass occurs in the time interval corresponding to 50-100 minutes after heating commences. This interval corresponds to particle growth up to a mean particle diameter of approximately 400 nm. Thereafter, the rate of mass growth appears to slow considerably. This phenomenon may arise from a number of mechanisms including exhaustion of particle formation precursors, settling effects, etc. In conjunction with concurrently acquired QCM mass deposition data, similar calculations for different samples and heating conditions may provide significant insight into the fundamental mechanisms and kinetics of particle formation and thermal degradation of jet fuels.

3. Conclusions

The primary responsibilities of Sandia National Laboratories in the Advanced, Thermally-Stable Jet Fuel Program are the development of instrumentation for monitoring jet fuel thermal stability characteristics, data acquisition, data interpretation and modeling, and transfer of technology to project participants. The major focus during the past year has been in instrumentation development and technology transfer. The static-flow jet fuel system

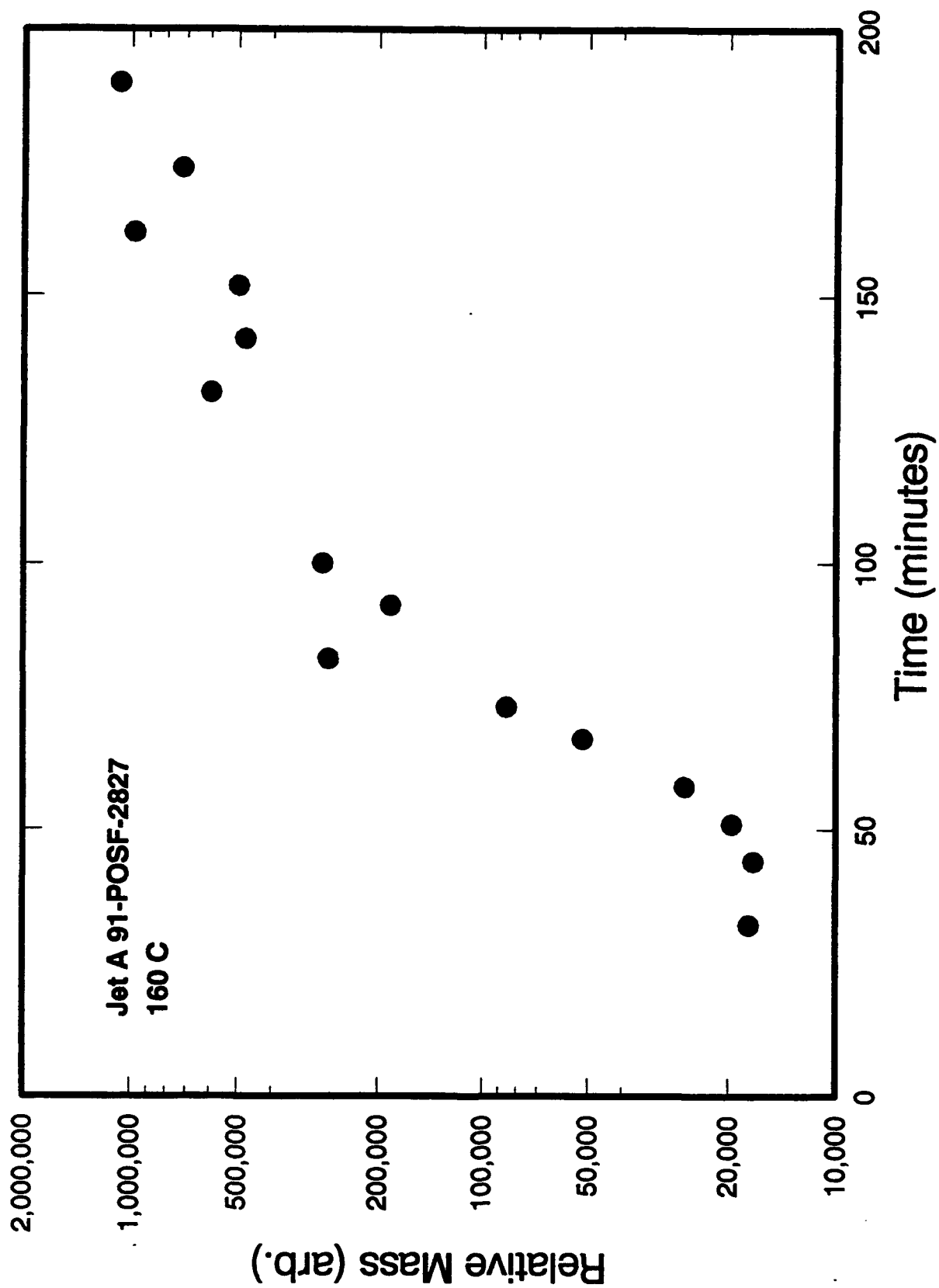


Figure 27. Relative mass of particles in Jet A 92-POSF-2827 heated to 160°C (see text for description of calculation method).

(QCM-JFTS) was completed and transferred to WL, UDRI, and Pratt & Whitney Corporation. The capabilities of the system were extended with regard to operating conditions and liquids that can be tested. A first-generation flow-thru system was developed and a second-generation system designed. An important aspect of the flow-thru system was the development of an algorithm and procedure to compensate the areal mass density values for fluctuations in temperature. Testing of that procedure is underway.

The PCS system is now being used at Wright Laboratory with work at Sandia focused on interpretation of data. Three fuels were systematically tested at Sandia and properties related to particle size formation and growth, induction times, mass of particles and particle size distributions were documented. Diffusion coefficients were measured for the three fuels at discrete temperatures. To enhance the quantification of the interpreted results, several software modifications were made and refractive index values of the fuels determined. Relative masses of particle sizes were calculated based on intensity measurements; these values are required to allow kinetic modeling.

An important accomplishment was the integration of the PCS and QCM technologies. Data from the integrated system was consistent with data from tests performed with the individual systems. A second-generation integrated system was designed and is being assembled. During the next year of activities, the integrated static-flow system technology is expected to be transferred to WL and an integrated QCM-PCS flow-thru system is expected to be made operational.

Bibliography

1. Berne, B. J. and Pecora, R., Dynamic Light Scattering with Applications to Chemistry, Biology and Physics, (Wiley, New York, 1976), Chapter 5.
2. Bohren, C. F. and Huffman, D. R., Absorption and Scattering of Light by Small Particles, (Wiley-Interscience, New York, 1983), pp. 477-482.
3. Bolshakov, G. F., "The Physico-Chemical Principles of the Formation of Deposits in Jet Fuels," Wright-Patterson AFB Report, AD-781 164, April 1974.
4. Heneghan, S. P. and Harrison, W. E., "Anti-Oxidants in Jet Fuels: A New Look," Proceedings of American Chemical Society Division of Petroleum Chemistry, Symposium of Structure of Jet Fuels, April 1992, pp. 404-411.

5. Klavetter, E., Trott, W., O'Hern, T., and Martin S., Advanced Thermally Stable, Jet Fuels Development Program Annual Report, Volume 1--Model and Experiment System Development, WL-TR-91-2099, January 1992.
6. Klavetter, E., Martin, S., Trott, W., O'Hern, T., Nelson, G., and Tallant, D., Advanced Thermally Stable, Coal-Derived, Jet Fuels Development Program Annual Report, Experiment System and Model Development, WL-TR-92-2105, February 1993.
7. O'Hern, T. J., Trott, W. M., Martin, S. J., and Klavetter, E. A., "Advanced Diagnostics for In Situ Measurement of Particle Formation and Deposition in Thermally Stressed Jet Fuels," 31st Aerospace Sciences Meeting and Exhibit, Reno, NV, Paper No. AIAA 93-0363, January 11-14, 1993.
8. Oliver, C. J., "Correlation Techniques," in Photon Correlation and Light Beating Spectroscopy, H. Z. Cummins and E. R. Pike, Eds. (Plenum, New York, 1974), pp. 151-223.
9. Trott, W. M., O'Hern, T. J., and Klavetter, E. A., "In Situ Measurement of Particle Formation in Heated Jet Fuels--A New Application of Photon Correlation Spectroscopy," Proceedings of American Chemical Society Division of Petroleum Chemistry, Symposium of Structure of Jet Fuels, April 1992, pp. 442-450.
10. Weiner, B.B., "Particle Sizing Using Photon Correlation Spectroscopy," in Modern Methods of Particle Size Analysis, H. G. Barth, Ed. (Wiley, New York, 1984), pp. 93-116.